

Award Number: W81XWH-09-1-0127

TITLE: The Role of the Omental Microenvironment in Ovarian Cancer Metastatic Colonization

PRINCIPAL INVESTIGATOR: Carrie W. Rinker-Schaeffer, Ph.D.

CONTRACTING ORGANIZATION: The University of Chicago
Chicago, IL 60637

REPORT DATE: August 2012

TYPE OF REPORT: Annual

PREPARED FOR: U.S. Army Medical Research and Materiel Command
Fort Detrick, Maryland 21702-5012

DISTRIBUTION STATEMENT: Approved for Public Release;
Distribution Unlimited

The views, opinions and/or findings contained in this report are those of the author(s) and should not be construed as an official Department of the Army position, policy or decision unless so designated by other documentation.

REPORT DOCUMENTATION PAGE				Form Approved OMB No. 0704-0188	
Public reporting burden for this collection of information is estimated to average 1 hour per response, including the time for reviewing instructions, searching existing data sources, gathering and maintaining the data needed, and completing and reviewing this collection of information. Send comments regarding this burden estimate or any other aspect of this collection of information, including suggestions for reducing this burden to Department of Defense, Washington Headquarters Services, Directorate for Information Operations and Reports (0704-0188), 1215 Jefferson Davis Highway, Suite 1204, Arlington, VA 22202-4302. Respondents should be aware that notwithstanding any other provision of law, no person shall be subject to any penalty for failing to comply with a collection of information if it does not display a currently valid OMB control number. PLEASE DO NOT RETURN YOUR FORM TO THE ABOVE ADDRESS.					
1. REPORT DATE August 2012		2. REPORT TYPE Annual		3. DATES COVERED 1 Aug 2011 – 31 Jul 2012	
4. TITLE AND SUBTITLE The Role of the Omental Microenvironment in Ovarian Cancer Metastatic Colonization				5a. CONTRACT NUMBER	
				5b. GRANT NUMBER W81XWH-09-1-0127	
				5c. PROGRAM ELEMENT NUMBER	
6. AUTHOR(S) Carrie Rinker-Schaeffer, Ph.D., Robert Clark, B.S., and Venkat Krishnan, Ph.D. E-Mail: crinkers@uchicago.edu "				5d. PROJECT NUMBER	
				5e. TASK NUMBER	
				5f. WORK UNIT NUMBER	
7. PERFORMING ORGANIZATION NAME(S) AND ADDRESS(ES) The University of Chicago Chicago, IL 60422				8. PERFORMING ORGANIZATION REPORT NUMBER	
9. SPONSORING / MONITORING AGENCY NAME(S) AND ADDRESS(ES) U.S. Army Medical Research and Materiel Command Fort Detrick, Maryland 21702-5012				10. SPONSOR/MONITOR'S ACRONYM(S)	
				11. SPONSOR/MONITOR'S REPORT NUMBER(S)	
12. DISTRIBUTION / AVAILABILITY STATEMENT Approved for Public Release; Distribution Unlimited					
13. SUPPLEMENTARY NOTES					
14. ABSTRACT In order to control ovarian cancer metastasis formation, there is significant interest in identifying the tissue microenvironments involved in cancer cell colonization of the omentum. Omental adipose is a site of prodigious metastasis in both ovarian cancer models and clinical disease. It is unusual as it contains milky spots, structures consisting of immune cells, stromal cells and structural elements surrounding glomerulus-like capillary beds. Contrary to studies reporting that omental colonization is adipocyte-driven, work presented herein shows that milky spots and adipocytes play distinct, complementary roles in omental metastatic colonization. Specifically, <i>in vivo</i> assays showed that ID8, CaOV3, HeyA8 and SKOV3ip.1 cancer cells preferentially lodge and grow within omental and splenoportal fat, which contain milky spots, as compared to other peritoneal fat depots. Similarly, media conditioned by milky spot-containing adipose tissue caused 75% more cell migration than media conditioned by milky spot-deficient adipose. Studies using a panel of immune-deficient mice showed that the mouse genetic background does not alter omental milky spot number and size, nor does it affect ovarian cancer colonization. Finally, consistent with the role for lipids as an energy source for cancer cell growth, <i>in vivo</i> time-course studies found an inverse relationship between metastatic burden and omental adipocyte content. Our findings provide new insights into the critical role milky spots play in omental metastatic colonization, the critical first step in the development of widespread peritoneal disease.					
15. SUBJECT TERMS Nothing Listed					
16. SECURITY CLASSIFICATION OF:			17. LIMITATION OF ABSTRACT	18. NUMBER OF PAGES	19a. NAME OF RESPONSIBLE PERSON
a. REPORT	b. ABSTRACT	c. THIS PAGE			USAMRMC
U	U	U	UU	70	19b. TELEPHONE NUMBER (include area code)

Table of Contents

Section	Page
<i>Introduction.....</i>	<i>2</i>
<i>Body.....</i>	<i>2</i>
<i>Key Research Accomplishments.....</i>	<i>3</i>
<i>Reportable Outcomes.....</i>	<i>3</i>
<i>Conclusions and Future Directions.....</i>	<i>12</i>
<i>References.....</i>	<i>15</i>
<i>Appendices.....</i>	<i>17</i>

Introduction: In order to more clearly define the functional role of milky spots and their components in metastatic colonization, we evaluated the lodging and progressive growth of ovarian cancer cells in peritoneal fat that either contains or lacks milky spots. *In vivo* studies using a panel of ovarian cancer cell lines showed that milky spots dramatically enhance early cancer cell lodging on peritoneal adipose tissues. Similarly, conditioned medium from milky spot-containing fat had a significantly increased ability to direct cell migration, compared with conditioned medium from milky spot-deficient fat. Studies using a panel of immunodeficient mice showed that the number and size of omental milky spots is not dependent on the mouse genetic background and, similarly, that ovarian cancer cell colonization does not depend on the immune composition of the milky spot. Finally, consistent with the role for lipids as an energy source for ovarian cancer cell growth, *in vivo* time-course studies revealed an inverse relationship between metastatic burden and omental adipocyte content.

Body: After escape from the primary tumor, ovarian cancer cells in the peritoneal fluid have access to and can potentially lodge within a variety of tissues (1,2). In both clinical disease and experimental models, however, the omentum is the site of prodigious metastasis formation (3-5). Thus, attachment of ovarian cancer cells to the omentum represents an early step in the development of widespread peritoneal disease (6,7). As the central regulator of peritoneal homeostasis, its functions include regulating fluid and solute transport, sensing and repairing injuries, promoting angiogenesis, fighting infection, serving as a source of stem cells, producing regulatory molecules, and storing and supplying lipids (8-12). These diverse functions are conferred by the cellular composition and architecture characteristic of human omenta.

Aside from the clear collagenous membrane that acts as a scaffold for the organ, the majority of the omentum is composed of bands of adipose tissue that contain adipocytes, blood and lymph vessels, immune cells, stromal cells, and connective matrix components that lie beneath an irregular mesothelium (8-12). In general, adipocytes have a variety of functions, ranging from lipid storage to production of endocrine molecules, and can serve as an integrating hub for inflammation, metabolism, and immunity (13-20). A distinctive feature of the omental vasculature is the presence of numerous branching blood vessels ending in tortuous glomerulus-like capillary beds near the tissue periphery (21-23). Immune cells aggregate around and within these capillary beds to form milky spots, which are the major immune structure for host defense of the peritoneal cavity (20, 25-36). In milky spots, both the endothelial lining of the capillaries and the overlying mesothelium are specially adapted to facilitate transmigration of immune cells (35). Additional structural elements include plasmocytes, fibroblasts, and mesenchymal cells, as well as collagen and reticular and elastic fibers (21).

A comprehensive literature review showed that studies examining the role of the omentum in metastasis focus on the contribution of its individual components, and not on the tissue as a whole. In our view, results from the majority of studies support models in which ovarian cancer metastatic colonization is driven either purely by milky spots or purely by adipocytes. The milky spot-driven model is based on a large body of *in vivo* data showing that, on intraperitoneal injection, cancer cells rapidly and specifically localize, invade, and proliferate within omental milky spots (36-40). In contrast, the adipocyte-driven model is based on studies published since the awarding of this grant. This model was prompted by the observation that, in its resting state, the omentum is composed predominantly of adipose and that cultured adipocytes can produce adipokines capable of promoting ovarian cancer cell migration and invasion *in vitro* (41). Adipocytes can also provide a proliferative advantage by transferring fatty acids to ovarian cancer cells (41). Although both models have clear strengths, neither addresses the intimate and dynamic interaction among milky spots, surrounding adipocytes, and other components of omental tissues.

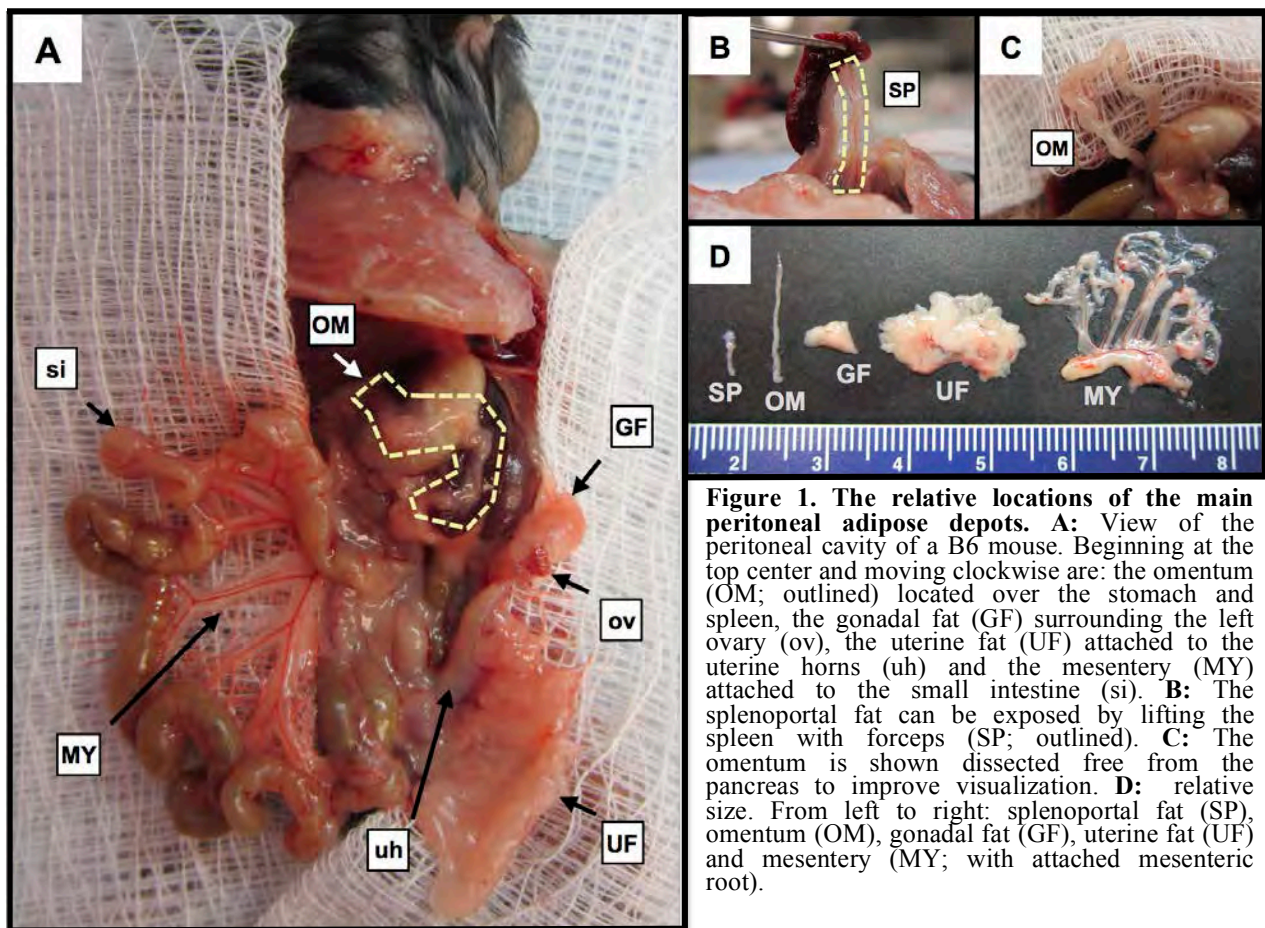
Key Research Accomplishments:

1. Identified both milky spot containing and deficient depots of peritoneal adipose to use to dissect that role(s) of milky spots and adipocytes in the promotion of ovarian cancer cell metastatic colonization.
2. Ovarian cancer cells preferentially colonize peritoneal adipose that contains milky spots.
3. Omental tissues secrete a factor(s) that can promote ovarian cancer cell migration.
4. Milky spot-containing tissues show enhanced ability to stimulate directed migration.
5. *In vivo* colonization of omental milky spots by ovarian cancer cells is not dependent on their immune cell composition.
6. During progressive growth ovarian cancer cells replace omental adipose.

Reportable Outcomes:

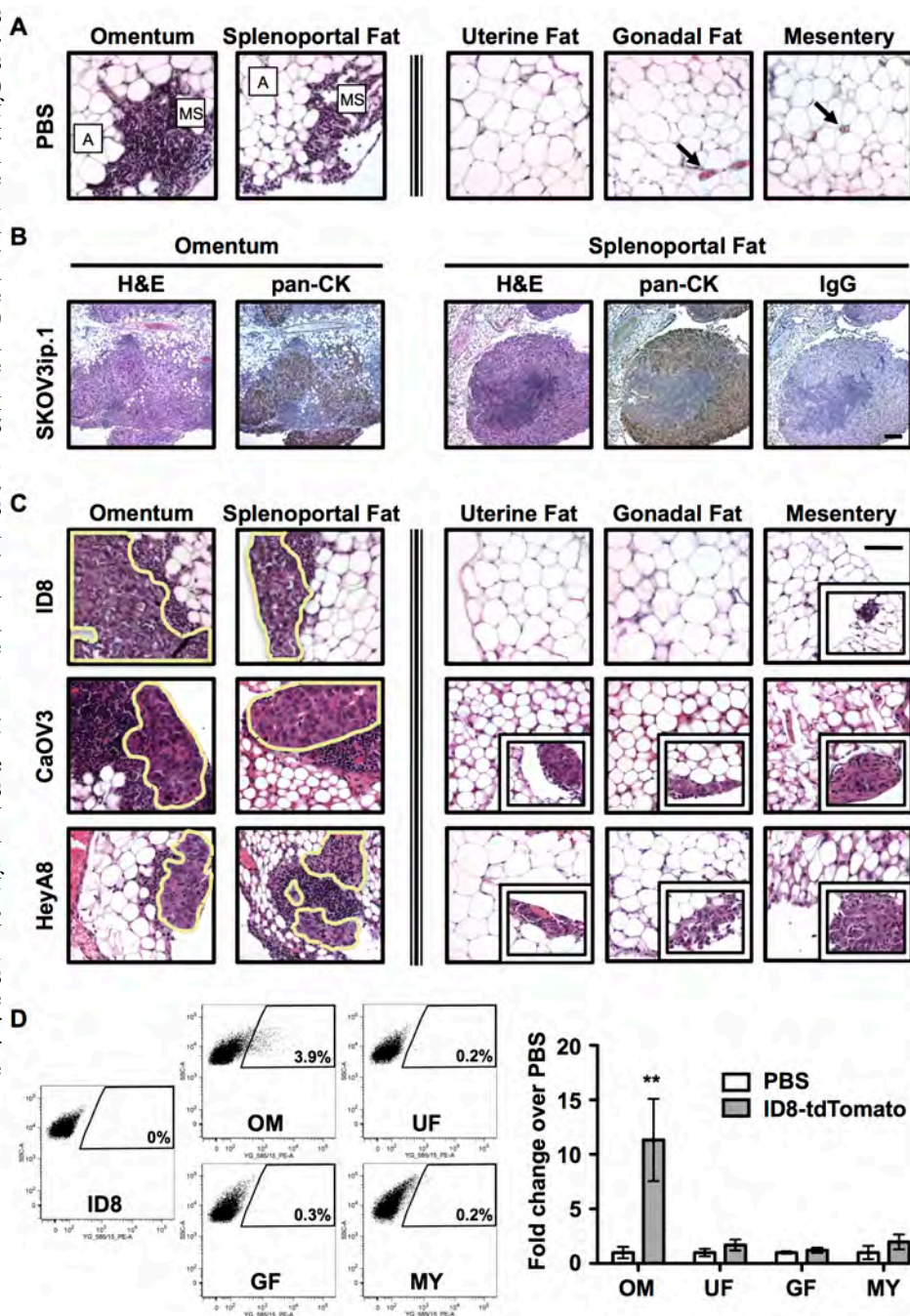
Several sources of adipose tissue are accessible to ovarian cancer cells in the peritoneal cavity.

There are five major adipose depot structures in the peritoneal cavity (2). As shown in Figure 1A, a lateral view of a ventral dissection allows visualization of the omentum (OM), gonadal fat (GF), uterine fat (UF), and mesentery (MY). The ovary (ov), uterine horn (uh) and small intestine (si) are indicated as points of reference. Further dissection allows for clear visualization of the splenoportal fat (SP), which surrounds the splenic artery and connects the hilum of the spleen to the celiac artery (Figure 1B), and the omentum, shown isolated from the pancreas (Figure 1C). The gross structure and relative size of these tissues is shown in Figure 1D.



Interestingly, in 1995 Takemori *et al*, reported the presence of milky spots in the splenoportal fat of New Zealand Black mice that are similar in structure and composition to omental milky spots; however, they did not examine cancer cell localization to these structures [42]. Consistent with their findings, we found that both the omentum and splenoportal fat have archetypal milky spot structures (Figure 2A). In contrast, these structures were not observed in uterine, gonadal and mesenteric fat (Figure 2A). Further, 7 days after i.p. injection of SKOV3ip.1 cells, comparable cancer cell lesions were observed in both omental and splenoportal fat (Figure 2B) and not other fat depots. IHC using a human pan-cytokeratin (pan-CK) antibody showed that the lesions were composed of SKOV3ip.1 cells intermingled with the immune cells. The specificity of IHC staining was confirmed by staining with an IgG control antibody (Figure 2B).

Figure 2. Ovarian cancer cells preferentially colonize peritoneal adipose that contains milky spots. **A:** Milky spots (MS) are observed in the adipose (A) of the omentum and splenoportal fat of PBS-injected and naïve mice. In contrast, no milky spots were detected in the uterine fat, gonadal fat and mesentery, each composed mostly of adipocytes. Representative data from PBS-injected B6 mice is shown. **Arrows** indicate blood vessels. Scale bar equals 50 μ m. **B.** Standard histology and IHC shows comparable colonization of milky spots in both omentum and splenoportal fat (after injection of 1×10^6 SKOV3ip.1 cells into Nude mice). Sections evaluated by H&E staining. Epithelial (cancer) cells within the lesions were confirmed by IHC for cytokeratin using a pan-cytokeratin (pan-CK) antibody. IHC using an IgG isotype antibody for pan-cytokeratin served as a control. The scale bar is the same for all images and denotes 100 μ m. **C.** Evaluation of ID8, CaOV3, and HeyA8 ovarian cancer colonization of peritoneal fat depots at 7 dpi. Cancer cell lesions are outlined. Representative examples of the cancer lesions occasionally seen in uterine, gonadal, and mesenteric fat are shown in insets. **D.** Flow cytometric analyses of omentum (OM), uterine fat (UF), gonadal fat (GF), and mesentery (MY) harvested from mice at 7 dpi of ID8-tdTomato cells. Data is presented as fold change increase of tdTomato-positive cells over PBS-injected mice (right). Error bars indicate standard error of the mean. ** denotes $p < 0.01$ compared to PBS controls.



Ovarian cancer cells preferentially colonize peritoneal adipose that contains milky spots. As described in the introduction, a review of the literature showed that ovarian cancer's predilection for omental metastasis formation can be ascribed to either adipose-driven or milky spot-driven mechanisms. However, these models are based upon studies focusing on either structural features (i.e. milky spots) or cellular components (i.e. adipocytes) of omental tissue (25,38,41). The availability of peritoneal fat depots that contain or lack milky spot structures enabled us to distinguish experimentally between the two models in the physiologically relevant setting of the peritoneal cavity. We reasoned that if colonization were purely adipocyte-driven, ovarian cancer cells would colonize the various peritoneal adipose depots to a similar extent after i.p. injection. In contrast, if milky spots drive this process, the omentum and splenoportal fat would have cancer cell foci in their numerous milky spots, while uterine, gonadal, and mesenteric fat would essentially be free of cancer cell colonies. Although our previous studies using SKOV3ip.1 cells support this latter model, studies using additional ovarian cancer cell lines are needed to determine the generalizability of these findings. To this end, the ability of ID8, CaOV3, and HeyA8 cells to form cancer cell foci on the five distinct peritoneal fat after i.p. injection into B6 (ID8) or Nude (CaOV3, HeyA8) mice was assessed by histology. The average number of cancer cells in a representative section of tissue was determined and expressed as foci/slide (Table 1). At 7 dpi, numerous large foci of ID8 cells were seen within the milky spots of both the omentum (ave. 48 foci/slide) and splenoportal fat (ave. 5 foci/slide) (Figure 2C). No ovarian cancer cells were detected in the uterine or gonadal fat (Figure 2C). In the mesentery, small clusters (<10 cells) of cancer cells were seen observed (ave. 2 foci/slide) on the tissue periphery (Figure 2C, *inset*). In agreement with these findings, CaOV3 cells showed similar pattern and extent of foci formation in the peritoneal adipose (Figure 2C, *inset*). Interestingly, HEYA8 cells had a greater ability to form surface foci on gonadal fat (UF) with 8 foci/slide (ave). [Figure 2C, *inset* (Table 1)].

Table 1. Histologic assessment of ID8, CAOV3, and HeyA8 colonization of peritoneal adipose depots

Mouse Strain	Cell Line	Tissue Type	Presence of Cancer Foci in Adipose Depot ^a	# Foci/Slide	Ave. # Foci/Slide
C57Bl/6	ID8	OM	5 / 5	36, 46, 50, 51, 58	48
		SP	5 / 5	3, 3, 6, 6, 6	5
		GF	0 / 5	0, 0, 0, 0, 0	0
		MY	5 / 5	1, 1, 1, 2, 4	2
		UF	0 / 5	0, 0, 0, 0, 0	0
Nude	CaOV3	OM	5 / 5	17, 19, 22, 23, 24	21
		SP	5 / 5	7, 7, 13, 13, 20	12
		GF	1 / 5	1, 0, 0, 0, 0	0
		MY	5 / 5	1, 2, 2, 4, 4	3
		UF	2 / 5	1, 1, 0, 0, 0	0
	HeyA8 ^b	OM	4 / 4	25, 27, 29, 35	29
		SP	4 / 4	6, 7, 8, 10	8
		GF	3 / 4	1, 1, 3, 0	1
		MY	4 / 4	1, 4, 6, 8	5
		UF	4 / 4	6, 6, 10, 11	8

^a Incidence of cancer foci in organ in each of 5 mice injected

^b HeyA8 mouse cohort n=4 due to mis-injection of an individual mouse

Finally, to complement our findings from our histological analyses and enable future studies, we developed a protocol to quantitate the number of cancer cells present in peritoneal adipose depots. ID8-tdTomato cells were prepared and injected i.p. into B6 mice. At 7 dpi, the adipose organs were harvested and dissociated into a single-cell suspension. The number of tdTomato cells present in the population of remaining cells (i.e. immune, endothelial, and mesothelial cells, fibroblasts, etc.) was quantified via flow cytometry as described in the Materials and Methods. It should be noted that splenoportal fat was excluded because its small size prohibited reliable cell recovery. As shown in Figure 2D, omental tissue preparations contained a significant population of tdTomato-positive cells. When quantified (Figure 2D, *right*), the omentum showed a ~ 12-fold increase in the number of ID8-tdTomato cells present over PBS-injected controls while there was no significant increase in cell preps

from the gonadal fat, uterine fat, or mesentery. These data support our histological finding that ovarian cancer cells preferentially colonize milky spot-containing adipose and provide an additional quantitative method for future studies by our laboratory and others.

Omental tissues secrete a factor(s) that can promote ovarian cancer cell migration. Ovarian cancer cells specifically localize to the omentum within minutes after i.p. injection (3, 6, 36). This suggests that omental tissue produces a factor(s) that promotes cancer cell homing; however, previous studies have only examined the contribution of isolated adipocytes (41). To address this gap in knowledge, we first tested the ability of omentum-conditioned media to promote directed cancer cell migration. Using a modification of our published method for *ex vivo* organ culture (6), omenta were excised and allowed to normalize in DMEM/F12 media containing 20% FCS for 24 hrs. Tissues were then rinsed with PBS, placed in serum-free DMEM/F12, and maintained for up to 5 days *ex vivo*. Tissue integrity was assessed both histologically by visually evaluating intact (round, continuous cell membrane) versus necrotic (stellate, discontinuous cell membrane) adipocytes and functionally by measuring the level of IL-6 in the conditioned media every 24 hrs. In agreement with our previously published studies (6), omental tissues did not show loss of integrity or function under these conditions (Figure 3).

After normalization in DMEM/F12 containing 20% FCS, omenta were rinsed with PBS and allowed to condition serum-free DMEM/F12 for 24 hrs (subsequently referred to as conditioned serum-free media; CSF). Omenta maintained in serum-free (SF) media are termed starved omenta (SOM). The combinations of omenta and media used as chemoattractants for the 6 hr migration assay are summarized in Figure 4A, upper panel, while representative membranes from the migration assays are shown in Figure 4A, lower panel. The number of cells that migrated to the lower side of the membrane was determined by summing the number of cells in each of 5 independent fields observed at 100x magnification.

Initial studies tested the ability of omenta harvested from CD1 mice to promote migration of both mouse ID8 and human SKOV3ip.1 cells (Figure 4B). CD1 CSF media served as a strong chemoattractant for both ID8 and SKOV3ip.1 cells, resulting in a greater than 150-fold increase in migration relative to SF media controls. To ensure that these results are not specific to omenta harvested from CD1 mice, CSF from B6 and Nude mouse omenta were also tested in their ability to promote ID8 and SKOV3ip.1 cell migration. As shown in Figure 4C, CSF prepared from B6 and Nude mouse omenta were a strong chemoattractant for ID8 cells, stimulating migration on a par with CD1-conditioned media (Figure 4B). Consistent with this finding, B6 and Nude CSF also stimulated equivalent levels of migration in SKOV3ip.1 cells. Interestingly, SKOV3ip.1 cells show a consistently lower level of migration than ID8 cells in response to media conditioned by omenta from CD1, B6, and Nude mice. Taken together, these experiments showed that intact omental tissue can be used as a starting point for efforts to identify one or more secreted factors that promote ovarian cancer cell homing to omental tissues.

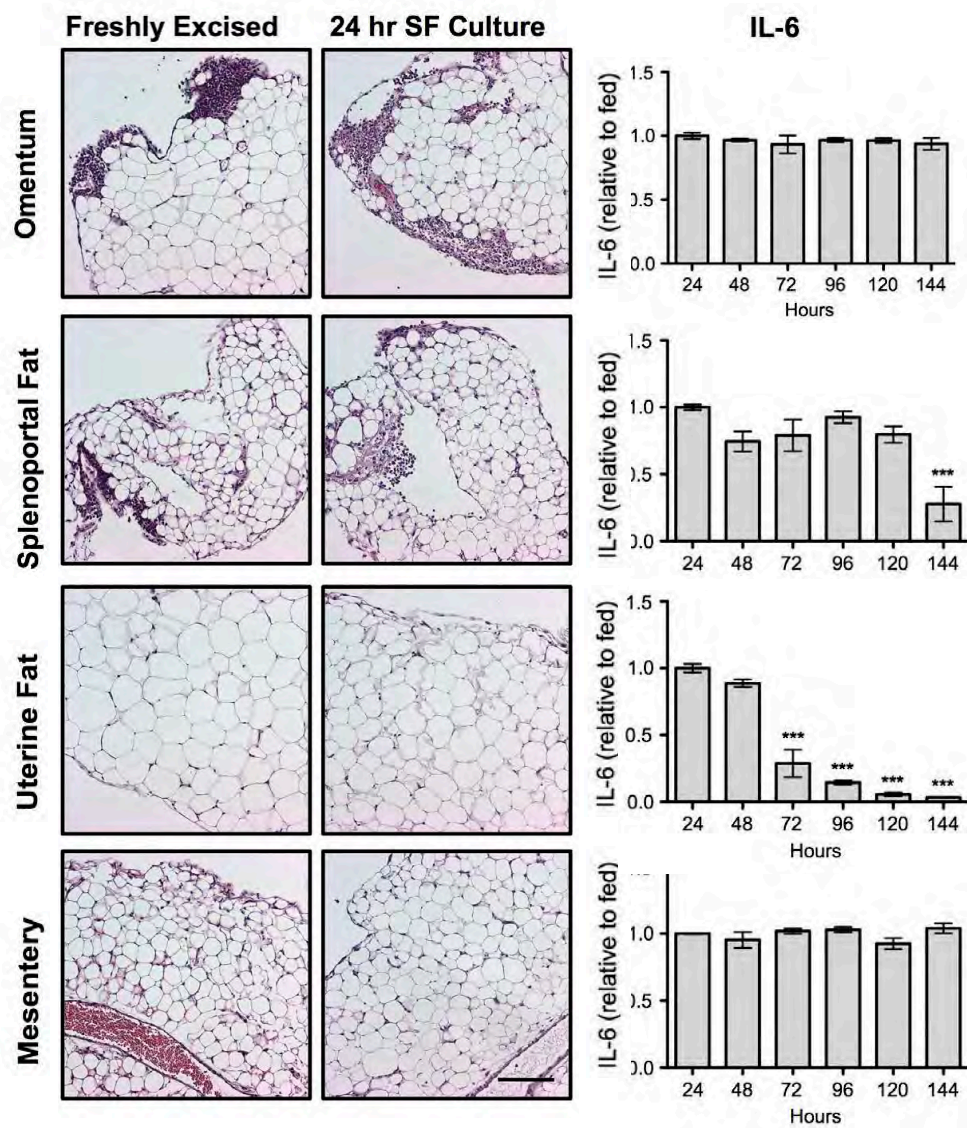


Figure 3. Evaluation of tissue integrity and function of tissues maintained in *ex vivo* culture. **Left column:** The appearance of freshly excised tissues. **Middle column:** Histology of tissues maintained for 24 hr in serum-free DMEM/F12. **Right column:** To assess tissue viability and function under *ex vivo* conditions, the amount of IL-6 in the SF culture media was determined at 24 hr intervals. As a control, the amount of IL-6 secreted by tissues maintained in media containing 20% FCS was determined in parallel. The relative amount of IL-6 at each timepoint is the ratio of the measured IL-6 concentration to the IL-6 concentration in the control group. The scale bar is the same for all images and denotes 50 μ m. Error bars indicate standard error of the mean, *** denotes $p < 0.001$.

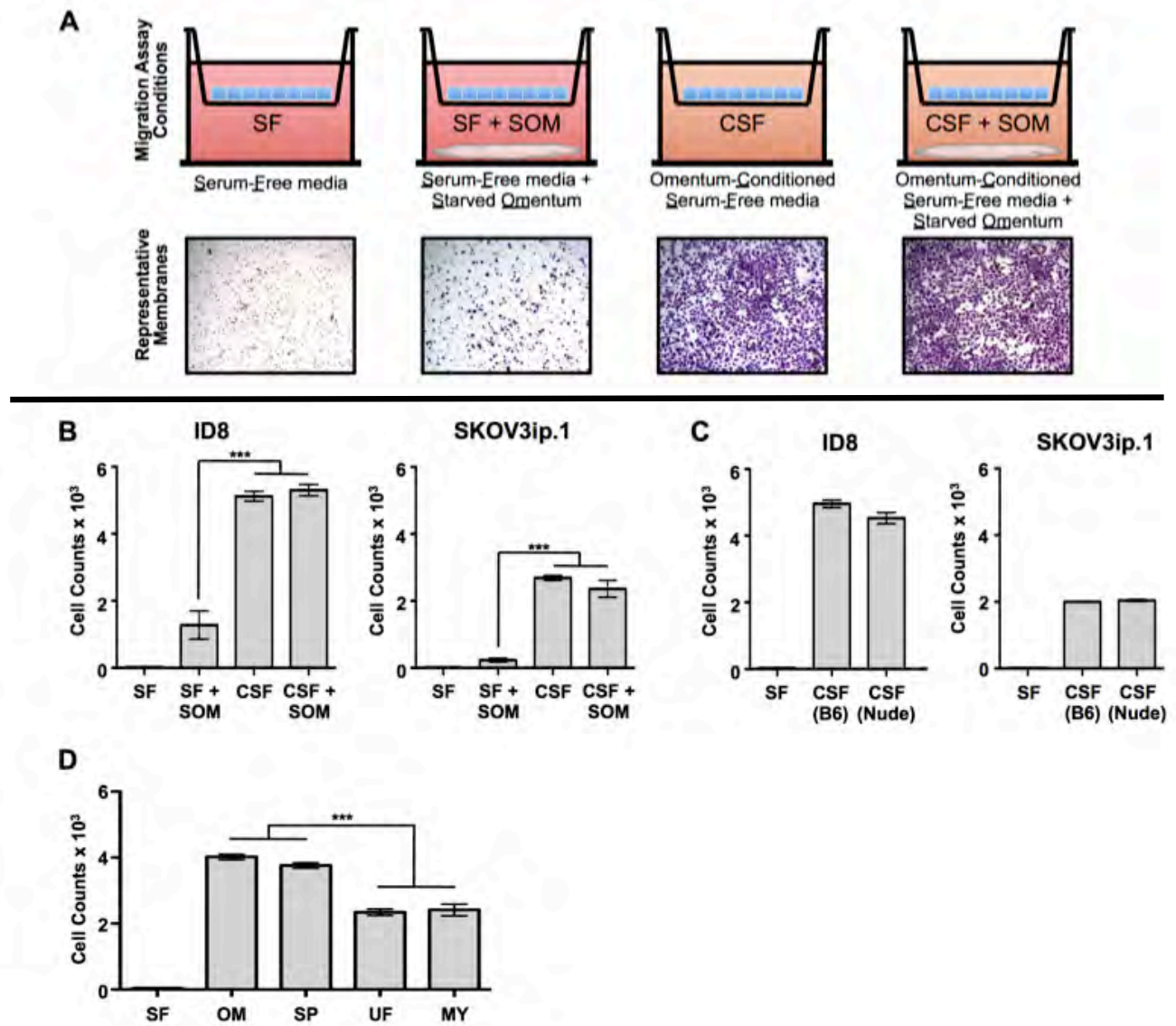


Figure 4. Milky spot-containing adipose tissues show enhanced ability to stimulate directed migration. **A:** *Top:* Depiction of migration assay setup. Cancer cells are placed in the upper chamber of the transwell apparatus. The chemoattractant media, with or without starved tissue, is placed in the lower chamber as indicated. *Bottom:* Representative membranes from ID8 migration assays. **B:** Quantitation of ID8 (*left*) and SKOV3ip.1 (*right*) cell migration in response to factors produced by omenta harvested from CD1 mice. Conditions are those illustrated in Panel A, where SF denotes serum free media where CSF denotes conditioned serum and SOM denotes starved omentum. **C:** Quantitation of ID8 (*left*) and SKOV3ip.1 (*right*) cell migration in response to media conditioned by omenta from either B6 or Nude mice [indicated as CSF(B6) and CSF(Nude), respectively]. **D:** Migration assay of ID8 cells toward serum-free media conditioned for 24 hr by tissue equivalents of omenta (OM), splenoportal fat (SP), uterine fat (UF) and mesentery (MY) harvested from B6 mice. n=5 for all conditions. Error bars indicate standard error of the mean, *** denotes p<0.001.

Milky spot-containing tissues show enhanced ability to stimulate directed migration. In their work, Nieman *et al.* showed that adipocytes cultured *in vitro* secreted cytokines that can promote migration of SKOV3ip.1 ovarian cancer cells (41). This raised the possibility that migration of cancer cells toward omentum-conditioned media could be a strictly adipose-driven process. If that were the case, we predicted that media conditioned by adipose tissue lacking milky spots would promote migration of ovarian cancer cells to the same extent as milky spot-containing adipose tissue. Alternatively, if milky spots play a key role in organ-specific homing, we expected that conditioned media from tissues containing milky spots could have an enhanced ability to promote migration. To distinguish between these possibilities, CSF media was prepared using weight-matched tissue equivalents of omentum, splenoportal fat, uterine fat, and mesentery and used as a chemoattractant in transwell migration assays. As shown in

Figure 3 tissues did not show loss of integrity or function for the duration of the migration assay. However, it was noted that the IL-6 production of the cultured uterine fat dropped significantly at 3 days in culture (Figure 3). The migration-promoting activity of CSF prepared from each of these tissues is summarized in Figure 4D. Media conditioned by omenta and splenoportal fat caused a 95-fold increase in cell migration as compared to SF media controls. In contrast, the absence of milky spots in uterine fat and mesentery corresponded with 75% reduction in the migration-stimulatory activity in their conditioned media (Figure 4D). Taken together, these functional studies bridge the adipocyte-driven and milky spot-driven models and argue that the presence of milky spots increases the chemoattractive potential of peritoneal fat depots.

***In vivo* colonization of omental milky spots by ovarian cancer cells is not dependent on their immune cell composition.** As a first step toward understanding the effect of the immune cell composition of milky spot structures on ovarian cancer cell colonization, experimental metastasis assays were conducted using immune competent (B6) and immunodeficient (Igh6, Nude, Rag1, and BN XID) mice. Specifically, 1×10^6 ID8 ovarian cancer cells were injected i.p. into all of the 5 different mouse strains. Cancer cell foci were observed within milky spots in each of these mouse strains at 7 dpi (Figure 5A) and were confirmed to be epithelial via positive staining for mouse cytokeratin 8/18 (CK8/18). To determine if the missing immune-cell types in the various immune-deficient mice alters cancer localization to milky spots, DAB area was quantified in CK8/18 stained sections. Figure 5B shows that ID8 cancer cells colonize omenta from each strain to a statistically equivalent degree. In parallel, 1×10^6 SKOV3ip.1 human ovarian cancer cells were injected into Nude, Rag1, and BN XID mice, and cancer foci were again found in each mouse strain (Figure 5C). SKOV3ip.1 lesions were stained for human pan-cytokeratin (pan-CK) and found to be cytokeratin-positive. Thus, ovarian cancer cell colonization of omental milky spots is not affected by deficiency or absence of T cells, B cells and/or NK cells in these mouse strains.

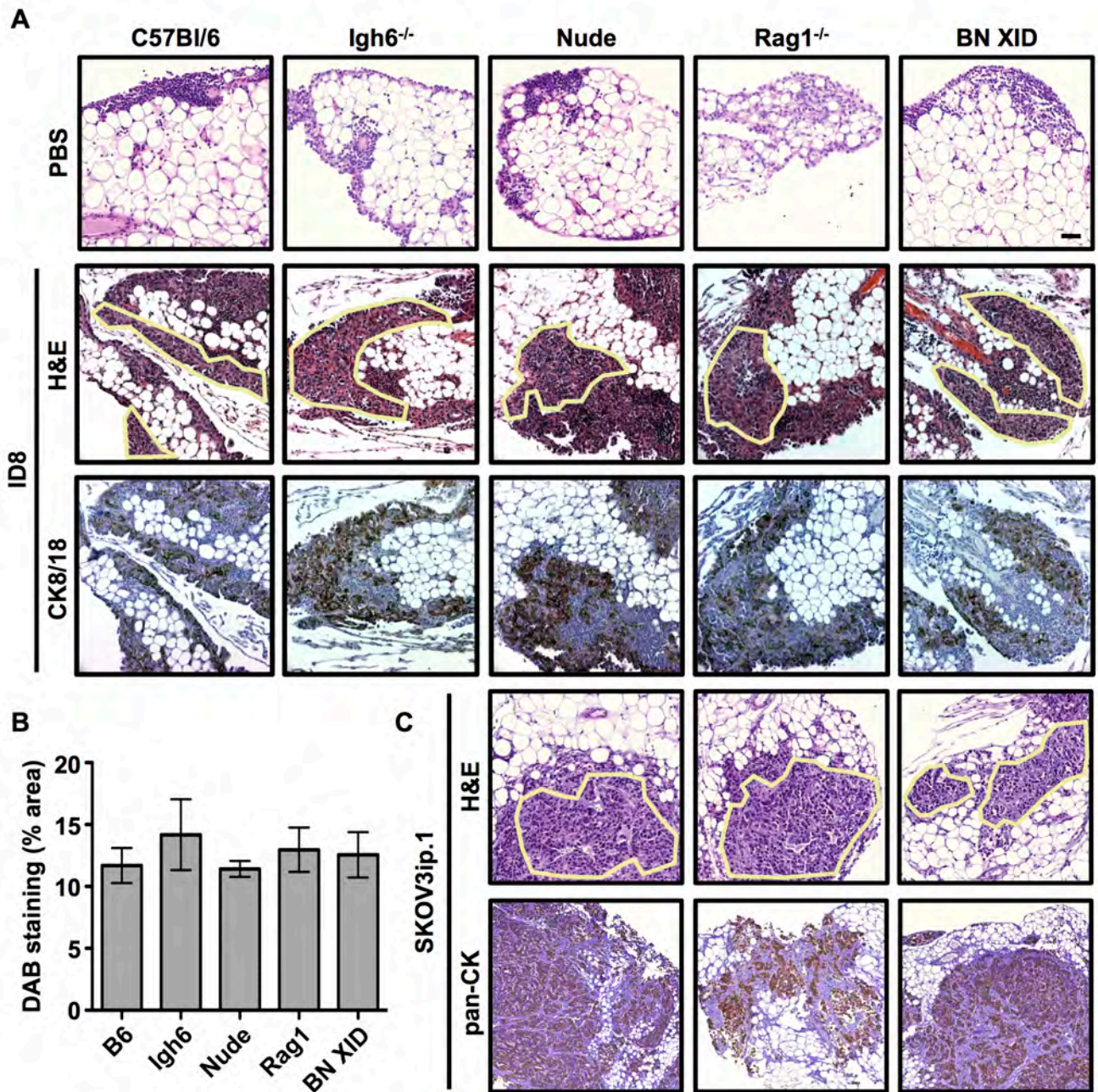


Figure 5. Colonization of omental milky spots by ovarian cancer cells is not dependent on the host immune status. To test the possibility that the immune composition of the milky spots has a quantitative effect on ovarian cancer cell colonization, mice with deficiencies in T cells, B cells and/or NK cells were injected i.p. with either PBS (control) or 1×10^6 ovarian cancer cells. **A:** B6, Igh6^{-/-}, Nude, Rag1^{-/-} and BN XID mice were injected with mouse ID8 cells (syngeneic to B6 background). Omenta were collected at 7 dpi and stained with H&E. Cancer cell foci within milky spots are outlined. IHC against mouse cytokeratin 8/18 (CK8/18) was used to confirm that the epithelial origin of the cancer cell foci. **B:** DAB staining area is used as an indicator of cancer cell burden in omental tissues. Values calculated as the percentage of ID8 with strong and medium intensity of CK8/18 (DAB) staining normalized to total stained area of the slide. Error bars indicate standard error of the mean. **C:** Human SKOV3ip.1 cells were injected into Nude, Rag1^{-/-} and BN XID mice and treated similarly to ID8 injected animals. IHC for against human pan-cytokeratin (pan-CK) was used to confirm the epithelial origin of cancer cell lesions. Samples from 5 independent animals were evaluated for each condition of each test. The scale bar is the same for all images and denotes 50 μ m.

During progressive growth ovarian cancer cells replace omental adipose. Mechanistic studies by Nieman *et al.* indicated that ovarian cancer cells could use adipocytes as an energy source for tumor growth (41). If this holds true *in vivo*, we predicted that as cancer cells proliferate, they interact with and consume adipocyte lipids. The ultimate outcome of this inverse relationship between cancer cell area and adipocyte area would be that, at the experimental endpoint, the omental adipose would be replaced completely with cancerous tissue. To test this notion, 1×10^6 ID8 ovarian cancer cells were injected i.p. into a cohort of B6 mice. Groups of 5 mice were euthanized and tissues collected for histologic analysis at 1, 3, 6 and 9 weeks post injection (Figure 6A). Consistent with an inverse relationship between ovarian cancer cell growth and adipocyte depletion, there is a marked reduction in the adipocyte area over time. To quantify this change, we used a pixel-based image processing protocol similar to milky spot quantification (detailed in the Materials and Methods) to calculate the adipocyte area in omenta over time. This showed a linear decrease in the percentage of adipocytes in the omentum corresponded to the expansion of ID8 cancer cell lesions (Figure 6B). These data are consistent with cancer cells' utilization of lipids stored in adipocytes as an energy source for their continued growth.

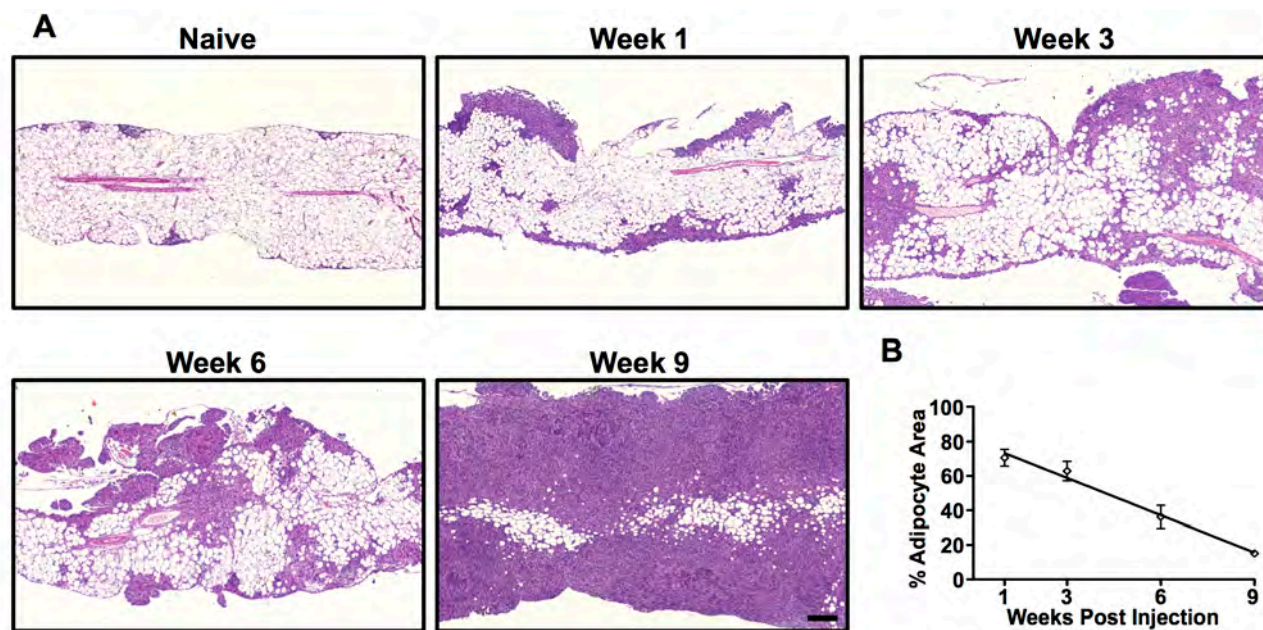


Figure 6. Adipocyte area of the omentum decreases during the timecourse ovarian cancer growth. **A:** The first panel shows a representative H&E stained section of an omentum from a naive B6 mouse. Milky spots are seen within adipose at the tissue periphery. The four subsequent panels show representative images of omental tissues harvested from B6 mice at 1, 3, 6 and 9 weeks post injection. The scale bar is the same for all images and denotes 200 μ m. **B:** Quantitation of adipocyte area from H&E images. Reported values are percent adipocyte area normalized to whole omental area. Data at each time point is based on five independent animals. Error bars indicate standard error of the mean. A linear regression of the data points indicates a slope significantly deviant from zero ($p < 0.0001$) with $R^2 = 0.8145$.

Conclusions and Future Directions:

There is now considerable literature on the structure and function of milky spots in both the omentum and extraomental sites. Beginning in the 1970s, investigators noted that ascites tumors had a proclivity for these structures (42). Subsequent studies have confirmed and refined these findings (3, 6, 36). The strength of this work is that it implies a functional role for milky spots in the early steps of omental colonization. However, the weakness of the “milky spot-driven” model prompted by this body of literature is that the studies on which it is based do not consider the potential contribution(s) of adipocytes and other cells within the omentum. While the failure to consider the contribution of

omental adipose in cancer metastasis is consistent with the now-antiquated view of adipocytes as an inert component of connective tissues (13, 18, 19), it is a fundamental oversight that must be addressed if we are to understand the organ specificity of ovarian cancer cells.

In contrast, the adipocyte-driven model prompted by the findings of Nieman *et al.*, showed that in omental metastases, ovarian cancer cells at the interface with adipocytes contained abundant lipids (41). *In vitro* studies showed that the adipocytes transfer lipid droplets that contain fatty acids to ovarian cancer cells (41), that can be used as an energy source. The strength of their studies is that they focused on human ovarian cancers and identified a novel function for adipocytes in the progressive growth of ovarian cancer lesions. The weakness of this work lies in its effort to show that adipocytes drive, and are solely responsible for, early steps in omental colonization. The case for adipose as the sole determinant of the ovarian cancer's organotropic metastasis was based on an incomplete examination of the literature and a biased approach to experimental design. As a result of the focus on adipocytes, important clues in the data were overlooked and the potential contributions of milky spots, vasculature, or other unique characteristics of the omentum were neither tested nor discussed. Thus, like the milky spot-driven model, this model is also limited by the narrow focus of the studies upon which it was based.

Despite their strengths, neither the milky spot-driven nor the adipocyte-driven models address the intimate and dynamic interactions among milky spot structures, adipocytes, and other omental components. Integration of these two models required a fresh look from a different perspective. Thus, we sought to understand why ovarian cancers *do not colonize* other sources of peritoneal fat as extensively as they do the omentum, rather than more traditional omentum-focused approaches. This led to our novel strategy to compare colonization of peritoneal adipose that either contains or lacks milky spots. The report by Takemori *et al* (42), showing the presence of milky spots in the splenoportal fat of New Zealand Black mice was key to our approach. To our knowledge, the splenoportal fat band has not been studied in other mouse strains, nor has its colonization by any type of cancer cells been examined prior to the work presented herein. *In vivo* studies using a panel of ovarian cancer cell lines (ID8, SKOV3ip.1, CaOV3, and HeyA8) yielded the most comprehensive assessment of ovarian cancer cell lodging in peritoneal adipose and provided clear data showing that milky spots dramatically enhance early cancer cell lodging.

To dissect the mechanism(s) by which milky spots promote colonization, we made use of the observation that after i.p. injection, ovarian cancer cells rapidly localize to omental milky spots, suggesting involvement of a tissue-secreted factor(s). Development of the quantitative transwell migration approach (Figure 4) enabled us to assess the ability of fat (tissue)-conditioned media to stimulate directed migration of ovarian cancer cells. Although milky spot-deficient tissues (uterine fat, gonadal fat and mesentery) secrete one or more factors that promotes directed migration, results from *in vivo* assays indicate that this signal is not sufficient for ovarian cancer cells to achieve the high level (both number and size) of foci formation seen in the omentum and splenoportal fat. This suggests that colonization requires additional chemotactic signals and/or tissue structures. In support of this notion, *in vivo* assays showed that ovarian cancer cells efficiently colonize milky spots in the omentum and splenoportal fat. In addition, using media conditioned by milky spot-containing adipose yielded the novel finding that the presence of these structures caused a significant enhancement in the media's ability to promote directed cancer migration.

Our findings show the critical importance of milky spots to ovarian cancer cell lodging and initial colonization of peritoneal adipose (3, 6, 21, 25, 36-40) and provide a foundation for studies to identify milky spot components involved in cancer cell homing and invasion. As a first step toward this goal, the use of immunodeficient mouse strains allowed us to rule out a requirement for B cells, T cells, or NK cells for ovarian cancer cell lodging within milky spots, confirming and expanding on the findings

of Lotan *et al.* (8) Previous studies have shown that mast cells and macrophages are frequently observed in the milky spots (27, 30, 31, 33). Macrophages are an intriguing candidate as they have been shown to assist the survival and growth of established tumors (43-45). Further, the depletion of peritoneal macrophages has been shown to decrease ovarian cancer tumor burden on the diaphragm at the experimental endpoint (46). Milky spot macrophages are thus possibly contributing to the rapid and specific colonization of omental milky spots. Another possible source of the omentum's chemotactic properties is the abundance of endothelial cells found in the milky spots. The vessels within the dense and tangled capillary bed of the milky spots have been shown to undergo a constitutive level of active vascular remodeling (25, 38). The activated endothelial cells associated with angiogenic vessels are known to support and promote metastatic disease (47, 48). Either or both of those cell types could be responsible for the prolific omental metastases and warrant future study.

The growing emphasis on the role of the host tissue microenvironment in metastasis formation stems from the seminal work of Stephen Paget showing that certain tumor cells (the "seed") have a proclivity for specific organ microenvironment(s) (the "soil") (49-51). A powerful but often underappreciated aspect of studies by Paget and other pioneers of metastasis research was their innate appreciation of the unique tissue architecture, physiology, and function of the target organ that is essential to understanding metastatic organ specificity (51-55). The studies presented herein seek to integrate milky spot and adipocyte function in the omentum. We propose a two-step model for omental colonization wherein the localization of disseminated cancer cells is dependent upon milky spots. Adipocytes are then required for progressive growth and subsequent spread of cancer cells to other sites within the peritoneal cavity. This model is likely a more accurate representation of the overall process of ovarian metastatic colonization. It is our hope that both our findings and discussion of the larger literature will serve as a framework for studies that will continue to refine our understanding of omental colonization. Ultimately, it is our goal to use this information to extend the duration of metastatic suppression and significantly increase the quality of life for patients diagnosed with ovarian cancer.

References:

1. Naora H, Montell DJ: Ovarian Cancer Metastasis: Integrating insights from disparate model organisms. *Nat Rev Cancer* 2005, 5:355–366.
2. Cinti S: The Adipose Organ. In: Fantuzzi G, mazzone T, editors. *Adipose Tissue and Adipokines in Health and Disease*, Totowa, New Jersey, Humana Press, 2007, pp. 3–19.
3. Hagiwara A, Takahashi T, Sawai K, Taniguchi H, Shimotsuma M, Okano S, Sakakura C, Tsujimoto H, Osaki K, Sasaki S: Milky spots as the implantation site for malignant cells in peritoneal dissemination in mice. *Cancer Research*, AACR, 1993, 53:687.
4. Roby KF, Taylor CC, Sweetwood JP, Cheng Y, Pace JL, Tawfik O, Persons DL, Smith PG, Terranova PF: Development of a syngeneic mouse model for events related to ovarian cancer. *Carcinogenesis* 2000, 21:585–591.
5. Lengyel E: Ovarian Cancer Development and Metastasis. *The American Journal of Pathology*, American Society for Investigative Pathology, 2010, 177:1053–1064.
6. Khan SM, Funk HM, Thiolloy S, Lotan TL, Hickson J, Prins GS, Drew AF, Rinker-Schaeffer CW: In vitro metastatic colonization of human ovarian cancer cells to the omentum. *Clin Exp Metastasis* 2010, 27:185–196.
7. Kenny HA, Krausz T, Yamada SD, Lengyel E: Use of a novel 3D culture model to elucidate the role of mesothelial cells, fibroblasts and extra-cellular matrices on adhesion and invasion of ovarian cancer cells to the omentum. *Int J Cancer* 2007, 121:1463–1472.
8. Liebermann-Meffert D: The greater omentum. *Anatomy, embryology, and surgical applications*. *Surg Clin North Am* 2000, 80:275–93–xii.
9. Collins D, Hogan AM, O'Shea D, Winter DC: The omentum: anatomical, metabolic, and surgical aspects. *J Gastrointest Surg* 2009, 13:1138–1146.
10. Platell C, Cooper D, Papadimitriou JM, Hall JC: The omentum. *World J Gastroenterol* 2000, 6:169–176.
11. Goldsmith HS: *The Omentum: Basic Research and Clinical Application*. 1st ed. Goldsmith HS, editor. New York, Cine Med, Inc, 1990.
12. Wilkosz S, Ireland G, Khwaja N, Walker M, Butt R, Giorgio-Miller A, Herrick SE: A comparative study of the structure of human and murine greater omentum. *Anat Embryol* 2005, 209:251–261.
13. Wozniak SE, Gee LL, Wachtel MS, Frezza EE: Adipose Tissue: The New Endocrine Organ? A Review Article. *Dig Dis Sci* 2008, 54:1847–1856.
14. Trayhurn P, Beattie JH: Physiological role of adipose tissue: white adipose tissue as an endocrine and secretory organ. *Proc Nutr Soc* 2001, 60:329–339.
15. Hauner H: The new concept of adipose tissue function. *Physiol Behav* 2004, 83:653–658.
16. Scherer PE: Adipose tissue: from lipid storage compartment to endocrine organ. *Diabetes* 2006, 55:1537–1545.
17. Kershaw EE, Flier JS: Adipose tissue as an endocrine organ. *J Clin Endocrinol Metab* 2004, 89:2548–2556.
18. Wang P, Mariman E, Renes J, Keijer J: The secretory function of adipocytes in the physiology of white adipose tissue. *J Cell Physiol* 2008, 216:3–13.
19. Conde J, Scotece M, Gómez R, López V, Gómez-Reino JJ, Lago F, Gualillo O: Adipokines: biofactors from white adipose tissue. A complex hub among inflammation, metabolism, and immunity. *Biofactors* 2011, 37:413–420.
20. Rajala MW, Scherer PE: Minireview: The adipocyte--at the crossroads of energy homeostasis,

inflammation, and atherosclerosis. *Endocrinology* 2003, 144:3765–3773.

21. Michailova KN, Usunoff KG: The milky spots of the peritoneum and pleura: structure, development and pathology. *Biomedical Reviews*, Varna, Bulgaria, 2004, 15:47–66.
22. Simer P: On the morphology of the omentum, with especial reference to its lymphatics. *American Journal of Anatomy*, Wiley Subscription Services, Inc., A Wiley Company, 1934, 54:203–228.
23. Ackermann PC, De Wet PD, Loots GP: Microcirculation of the rat omentum studied by means of corrosion casts. *Acta Anat (Basel)* 1991, 140:146–149.
24. Shimotsuma M, Shields J, Simpson-Morgan M, Sakuyama A, Shirasu M, Hagiwara A, Takahashi T: Morpho-physiological function and role of omental milky spots as omentum-associated lymphoid tissue (OALT) in the peritoneal cavity. *Lymphology* 1993, 26:90.
25. Gerber SA, Rybalko VY, Bigelow CE, Lugade AA, Foster TH, Frelinger JG, Lord EM: Preferential Attachment of Peritoneal Tumor Metastases to Omental Immune Aggregates and Possible Role of a Unique Vascular Microenvironment in Metastatic Survival and Growth. *The American Journal of Pathology*, American Society for Investigative Pathology, 2006, 169:1739–1752.
26. Shimotsuma M, Kawata M, Hagiwara A, Takahashi T: Milky spots in the human greater omentum. Macroscopic and histological identification. *Acta Anat (Basel)* 1989, 136:211–216.
27. Shimotsuma M, Simpson-Morgan MW, Takahashi T, Hagiwara A: Activation of omental milky spots and milky spot macrophages by intraperitoneal administration of a streptococcal preparation, OK-432. *Cancer Research* 1992, 52:5400–5402.
28. Litbarg NO, Gudehithlu KP, Sethupathi P, Arruda JAL, Dunea G, Singh AK: Activated omentum becomes rich in factors that promote healing and tissue regeneration. *Cell Tissue Res* 2007, 328:487–497.
29. Rangel-Moreno J, Moyron-Quiroz JE, Carragher DM, Kusser K, Hartson L, Moquin A, Randall TD: Omental Milky Spots Develop in the Absence of Lymphoid Tissue-Inducer Cells and Support B and T Cell Responses to Peritoneal Antigens. *Immunity*, Elsevier Ltd, 2009, 30:731–743.
30. Wijffels JF, Hendrickx RJ, Steenbergen JJ, Eestermans IL, Beelen RH: Milky spots in the mouse omentum may play an important role in the origin of peritoneal macrophages. *Res Immunol* 1992, 143:401–409.
31. Shimotsuma M, Takahashi T, Kawata M, Dux K: Cellular subsets of the milky spots in the human greater omentum. *Cell Tissue Res* 1991, 264:599–601.
32. Cranshaw ML, Leak LV: Milky spots of the omentum: a source of peritoneal cells in the normal and stimulated animal. *Arch Histol Cytol* 1990, 53 Suppl:165–177.
33. Beelen RH, Fluitsma DM, Hoefsmit EC: The cellular composition of omentum milky spots and the ultrastructure of milky spot macrophages and reticulum cells. *J Reticuloendothel Soc* 1980, 28:585–599.
34. Krist LF, Eestermans IL, Steenbergen JJ, Hoefsmit EC, Cuesta MA, Meyer S, Beelen RH: Cellular composition of milky spots in the human greater omentum: an immunochemical and ultrastructural study. *Anat Rec* 1995, 241:163–174.
35. Mironov VA, Gusev SA, Baradi AF: Mesothelial stomata overlying omental milky spots: scanning electron microscopic study. *Cell Tissue Res* 1979, 201:327–330.
36. Krist LF, Kerremans M, Broekhuis-Fluitsma DM, Eestermans IL, Meyer S, Beelen RH: Milky spots in the greater omentum are predominant sites of local tumour cell proliferation and accumulation in the peritoneal cavity. *Cancer Immunol Immunother* 1998, 47:205–212.
37. Green JA, Williams AE: The relationship between inflammatory responses and WBP1 tumour cell attachment to the rat omentum. *Eur J Cancer* 1978, 14:1153–1155.

38. Sorensen EW, Gerber SA, Sedlacek AL, Rybalko VY, Chan WM, Lord EM: Omental immune aggregates and tumor metastasis within the peritoneal cavity. *Immunol Res* 2009, 45:185–194.
39. Tsujimoto H, Takhashi T, Hagiwara A, Shimotsuma M, Sakakura C, Osaki K, Sasaki S, Shirasu M, Sakakibara T, Ohyama T: Site-specific implantation in the milky spots of malignant cells in peritoneal dissemination: immunohistochemical observation in mice inoculated intraperitoneally with bromodeoxyuridine-labelled cells. *Br J Cancer, Nature Publishing Group*, 1995, 71:468.
40. Tsujimoto H, Hagiwara A, Shimotsuma M, Sakakura C, Osaki K, Sasaki S, Ohyama T, Ohgaki M, Imanishi T, Yamazaki J, Takahashi T: Role of milky spots as selective implantation sites for malignant cells in peritoneal dissemination in mice. *J Cancer Res Clin Oncol* 1996, 122:590–595.
41. Nieman KM, Kenny HA, Penicka CV, Ladanyi A, Buell-Gutbrod R, Zillhardt MR, Romero IL, Carey MS, Mills GB, Hotamisligil GS, Yamada SD, Peter ME, Gwin K, Lengyel E: Adipocytes promote ovarian cancer metastasis and provide energy for rapid tumor growth. *Nat Med* 2011, 17:1498–1503.
42. Takemori N, Hirai K, Onodera R, Saito N, Namiki M: Light and electron microscope study of splenoportal milky spots in New Zealand black mice: comparison between splenoportal milky spots and aberrant spleens. *J Anat* 1995, 186 (Pt 2):287–299.
43. Qian B-Z, Pollard JW: Macrophage diversity enhances tumor progression and metastasis. *Cell* 2010, 141:39–51.
44. Tlsty TD, Coussens LM: Tumor stroma and regulation of cancer development. *Annu Rev Pathol* 2006, 1:119–150.
45. Coussens LM, Werb Z: Inflammation and cancer. *Nature* 2002, 420:860–867.
46. Robinson-Smith TM, Isaacssohn I, Mercer CA, Zhou M, Van Rooijen N, Husseinazadeh N, McFarland-Mancini MM, Drew AF: Macrophages Mediate Inflammation-Enhanced Metastasis of Ovarian Tumors in Mice. *Cancer Research* 2007, 67:5708–5716.
47. Orr FW, Wang HH, Lafrenie RM, Scherbarth S, Nance DM: Interactions between cancer cells and the endothelium in metastasis. *J Pathol, Wiley Online Library*, 2000, 190:310–329.
48. Chouaib S, Kieda C, Benlalam H, Noman MZ, Mami-Chouaib F, Rüegg C: Endothelial cells as key determinants of the tumor microenvironment: interaction with tumor cells, extracellular matrix and immune killer cells. *Crit Rev Immunol* 2010, 30:529–545.
49. Paget S: The distribution of secondary growths in cancer of the breast. 1889. *The Lancet* 1889, 133:571–573.
50. Kenny PA, Bissell MJ: Tumor reversion: correction of malignant behavior by microenvironmental cues. *Int J Cancer* 2003, 107:688–695.
51. Bissell MJ, Radisky DC, Rizki A, Weaver VM, Petersen OW: The organizing principle: microenvironmental influences in the normal and malignant breast. *Differentiation* 2002, 70:537–546.
52. Nicolson GL: Organ specificity of tumor metastasis: role of preferential adhesion, invasion and growth of malignant cells at specific secondary sites. *Cancer Metastasis Rev* 1988, 7:143–188.
53. Fidler IJ: The pathogenesis of cancer metastasis: the “seed and soil” hypothesis revisited. *Nat. Rev. Cancer*. 2003, pp. 453–458.
54. Hart IR, Fidler IJ: Role of Organ Selectivity in the Determination of Metastatic Patterns of B16 Melanoma. *Cancer Research* 1980.
55. Sugarbaker EV: Cancer metastasis: a product of tumor-host interactions. *Curr Probl Cancer* 1979, 3:1–59.

Appendices: Manuscript Submitted



Chicago, IL 60637-1470

DEPARTMENT OF SURGERY

Section of Urology

5841 South Maryland Avenue

Phone: (773) 702-5882

Lab: (773) 702-3140

Fax: (773) 702-1001

Carrie W. Rinker-Schaeffer, Ph.D.

Full Professor

Director of Urology Research

September 24, 2012

Michael P. Lisanti, M.D., Ph.D.,
Editor in Chief, *The American Journal of Pathology*,
9650 Rockville Pike, Bethesda,
Maryland, USA 20814-3993.

Dear Dr. Lisanti

Enclosed please find our manuscript, "Milky spots are required for ovarian cancer colonization of peritoneal adipose depots" submitted by Clark and Krishnan *et al.*, for consideration for publication in **The American Journal of Pathology**, as a **Research Article**. We believe that this work is ideally suited for your Journal as it focuses on the role of omental tissue composition and architecture in the pathological process of ovarian cancer metastatic colonization. It also presents a scholarly appraisal of omental tissue physiology and function and its potential contributions to ovarian cancer metastasis, which sadly has been overlooked by the ovarian cancer community. Consistent with the Journal's mission, this work will advance our basic and translational knowledge of ovarian cancer metastasis formation. The work uses physiologically relevant experimental models, and a combination of cellular, molecular, animal, and immunological approaches in conjunction with tissue morphology.

Work in this manuscript seeks to understand the role of the tissue microenvironment(s) in ovarian cancer cell lodging and progressive growth within the omentum, a preferred site of ovarian cancer metastasis formation. The omentum's tissue architecture is unusual in that its adipocyte-rich regions contain milky spots, structures consisting of immune cells, stromal cells and structural elements surrounding glomerulus-like capillary beds. Contrary to previous reductionist studies, our findings show that both milky spots and adipocytes play distinct, complementary roles in metastasis.

Specifically, metastasis assays using ID8 and SKOV3ip.1 ovarian cancer cells, showed that cells only lodge and grow within omental and splenoportal fat, which contain milky spots, and not other peritoneal fat depots. Similarly, media conditioned by milky spot-containing adipose tissue caused 72% more cell migration than media conditioned by milky spot-deficient adipose. Studies using a panel of immune-deficient mice showed that the

mouse genetic background does not alter omental milky spot number and size, nor does it effect ovarian cancer colonization. Finally, consistent with the role for lipids as an energy source for cancer cell growth, *in vivo* time-course studies found an inverse relationship between metastatic burden and omental adipocyte content. Our findings support a two-step model wherein both milky spots and adipose have specific roles in colonization of the omentum by ovarian cancer cells.

On behalf of the authors I can affirm that we have no financial conflict of interests to declare. I can also affirm that the manuscript has not been published previously and is not being considered concurrently by another publication, and affirm that all authors and acknowledged contributors have read and approved the manuscript. We cite a scientific conflict with Dr. Ernst Lengyel M.D., Department of Obstetrics and Gynecology, The University of Chicago. To facilitate the review process we have suggested members of the Editorial Board and larger scientific community that we believe are appropriate for the review of this manuscript. Please feel free to contact me if I can be of further assistance in this review process. Thank you in advance for your efforts on our behalf.

Most Sincerely,

A handwritten signature in black ink, appearing to read 'Carrie', followed by a horizontal line.

Carrie Rinker-Schaeffer, Ph.D.
President of the Metastasis Research Society
Departments of Surgery and Obstetrics and Gynecology
Committee of Cancer Biology
Committee on Genetics, Genomics and Systems Biology

Dr. Deborah Armstrong, Director Breast and Ovarian Surveillance Service

Johns Hopkins Sidney Kimmel Comprehensive Cancer Center

The Bunting-Blaustein Cancer Research Building-1

1650 Orleans Street, Room 190

Baltimore, Maryland 21231-1000

Tel: 410.614.2743 **Fax:** 410.955.0125 **Email:** armsrde@jhmi.edu

Dr. Ann Chambers, Distinguished Oncology Scientist

London Regional Cancer Program

Room A4-903b

790 Commissioners Rd. E.

London, Ontario

Canada N6A 4L6

Tel: **Fax:**

Email: Ann.Chambers@lhsc.on.ca

Dr. Victoria Seewaldt, Professor

Leader Breast and Ovarian Cancer Program

Duke University Comprehensive Cancer Center

Department of Medicine

Rm 221A MSRB

DUMC 2628

Durham, NC 27710

Tel: **Fax:**

Email: seewa001@mc.duke.edu

Dr. Patricia Steeg, Chief, Women's Cancers Section

Laboratory of Molecular Pharmacology

Center for Cancer Research, National Cancer Institute

Building 37, Room 1122

Bethesda, MD 20892

Tel:

Fax:

Email: steegp@mail.nih.gov

Dr. Ann Thor, Professor and Chair, Department of Pathology

University of Colorado Denver, School of Medicine

Department of Pathology

12631 E 17th Avenue, Room L15-2215

Mail Stop B216

Aurora, CO 80045

Tel: **Fax:** **Email:** Ann.Thor@ucdenver.edu

Milky spots are required for ovarian cancer colonization of peritoneal adipose depots

Robert Clark^{1,&}, Venkatesh Krishnan^{2,&}, Michael Schoof^{2,§}, Irving Rodriguez^{2,§}, Betty Theriault³, Marina Chekmareva⁴ and Carrie Rinker-Schaeffer^{2,#}

¹Department of Molecular Pathogenesis and Molecular Medicine, The University of Chicago, Chicago, IL

²The Section of Urology, Department of Surgery, The University of Chicago, Chicago, IL

³Department of Surgery and the Animal Resources Center, The University of Chicago, Chicago, IL

⁴Department of Pathology, Robert Wood Johnson Medical School, New Brunswick, NJ

[&]Authors contributed equally to this work

[§]Current address: Department of Natural Sciences, Stanford University, Stanford, CA

[#] To whom correspondence should be addressed:

Section of Urology, Department of Surgery, MC6038

The University of Chicago

5841 South Maryland Avenue

Chicago, IL 60637

Tel: 773-702-5882

Fax: 773-702-1001

Email: crinkers@uchicago.edu

Number of Text Pages: 42

Number of Tables: 0

Number of Figures: 7 Primary; 4 Supplemental

Short Running Title: Ovarian cancer colonizes milky spots

Financial Support

Work was supported by grants from the DOD (W81XWH-09-1-0127), NCI/NIH (2RO1CA089569), and Elsa U. Pardee Foundation; Marsha Rivkin Center for Ovarian Cancer Research Pilot Study Award; and funds from the Section of Urology (The University of Chicago)

Keywords: ovarian cancer, omentum, milky spots, peritoneal fat, splenoportal fat

45 **Abstract**

46 Control of ovarian cancer metastasis formation requires identification and understanding
47 of the specific tissue microenvironments involved in cancer cell colonization of the omentum.
48 Omental adipose is a site of prodigious metastasis in both ovarian cancer models and clinical
49 disease. It is unusual as its adipocyte-rich regions contain milky spots, structures consisting
50 of immune cells, stromal cells and structural elements surrounding glomerulus-like capillary
51 beds. Contrary to previous reductionist studies, work presented herein shows that milky spots
52 and adipocytes play distinct, complementary roles in metastasis. Specifically, metastasis
53 assays using ID8 and SKOV3ip.1 ovarian cancer cells showed that cells only lodge and grow
54 within omental and splenoportal fat, which contain milky spots, and not other peritoneal fat
55 depots. Similarly, media conditioned by milky spot-containing adipose tissue caused 75%
56 more cell migration than media conditioned by milky spot-deficient adipose. Studies using a
57 panel of immunodeficient mice showed that the mouse genetic background does not alter
58 omental milky spot number and size, nor does it affect ovarian cancer colonization. Finally,
59 consistent with the role for lipids as an energy source for cancer cell growth, *in vivo* time-
60 course studies found an inverse relationship between metastatic burden and omental
61 adipocyte content. Our findings support a two-step model wherein both milky spots and
62 adipose have specific roles in colonization of the omentum by ovarian cancer cells.

63

64 **Introduction**

65 It is estimated that in 2012 nearly 23,000 American women will be diagnosed with ovarian
66 cancer and 16,000 will die of their disease.¹ The majority of patients present with metastasis
67 or eventually succumb to metastatic disease within the abdominal cavity.¹ After escape from
68 the primary tumor, ovarian cancer cells populate the peritoneal fluid and have access to and
69 can potentially lodge within a variety of tissues.^{2,3} However, in both clinical disease and
70 experimental models, the omentum is a site of prodigious metastasis formation.⁴⁻⁷ Thus,
71 attachment of ovarian cancer cells to the omentum represents a rate-limiting step in
72 metastasis formation.^{8,9} Although the importance of the omentum is widely acknowledged,
73 there still is no consensus on the role its microenvironment plays in ovarian cancer
74 metastasis formation. This raises the question, “How do ovarian cancer cells specifically
75 colonize the omental tissue microenvironment?”

76 Studies of omental function date back to Jobert de Lamballe, a military surgeon to
77 Napoleon I, who was reportedly the first to recognize its curious ability to fight infection and
78 form adhesions to help control injuries.¹⁰ As a result of nearly two centuries of investigation, a
79 great deal is known about the omentum’s physiology and surgical applications.¹⁰⁻¹³ As the
80 central regulator of peritoneal homeostasis, its functions include: regulating fluid and solute
81 transport, sensing and repairing injuries, promoting angiogenesis, fighting infection, serving
82 as a source of stem cells, production of regulatory molecules and storing and supplying lipids.
83 Remarkably, these diverse functions are conferred by the interaction of the two structurally
84 distinct tissue types that compose it. The *translucent membranes* are composed of collagen
85 fibers and fibroblast-like cells enclosed by two closely opposed mesothelial cell layers that
86 assemble into a net-like structure with large fenestrations throughout.^{14,15} The fenestrations

87 are thought to be involved in both fluid transport and adhesion formation. A role for this tissue
88 in metastatic colonization has not been reported.

89 In contrast, the *adipose-rich areas* are composed of adipocytes, immune cells, stromal
90 cells and connective matrix components that lay beneath an irregular mesothelium.
91 Adipocytes have a variety of functions, ranging from lipid storage to production of endocrine
92 molecules.^{3,16-21} The adipose can also serve as an integrating hub for inflammation,
93 metabolism and immunity.²²⁻²⁵ A distinctive feature of the vasculature in omental adipose is
94 the presence of numerous branching blood vessels ending in tortuous glomerulus-like
95 capillary beds near the tissue periphery.²⁶⁻³⁰ Immune cells aggregate around and within these
96 glomeruli to form milky spots: the major immune structure for host defense of the peritoneal
97 cavity.^{26,31-38} In most milky spots, both the endothelial lining of the omental capillaries and the
98 overlying mesothelium are specially adapted to facilitate transmigration of immune
99 cells.^{26,39,40} Additional structural elements include plasmocytes, fibroblasts and mesenchymal
100 cells, as well as collagen, reticular and elastic fibers.^{31,36,39,41}

101 A comprehensive literature review showed that studies examining omental metastasis take
102 a reductionist approach and focus on the role of individual components of the adipose-rich
103 region. In our view, results from the majority of studies support models in which ovarian
104 cancer metastatic colonization is either purely “milky spot-driven” or purely “adipocyte-driven.”
105 The milky spot-driven model is based on a large body of *in vivo* data showing that after i.p.
106 injection, cancer cells rapidly and specifically localize to, invade and proliferate within omental
107 milky spots.^{4,7,26,30,42-46} An implication of this model is that cells within milky spots produce
108 chemotactic factors potentially responsible for cancer cell homing to and invasion of milky
109 spots, as well as provide a conducive microenvironment for cancer cell survival and
110 growth.^{30,34,42} In contrast, the adipocyte-driven model is based on the observation that in its

111 resting state, the omentum is predominantly composed of adipose. Furthermore, cultured
112 adipocytes can produce adipokines capable of promoting ovarian cancer cell migration and
113 invasion *in vitro*.⁴⁷ Additional studies showed that adipocytes could also provide a proliferative
114 advantage by transferring fatty acids to ovarian cancer cells.⁴⁷ Although there are clear
115 strengths to both of these models, neither addresses the intimate and dynamic interaction
116 between milky spot structures, adipocytes and other components of the adipose-rich region.

117 Using tissue architecture and function as a guide, we propose that an alternative, more
118 fully integrated model of metastatic colonization is needed. To test this we identified
119 peritoneal fat deposits (omentum, mesentery, uterine, gonadal and splenoportal fat) that are
120 accessible to ovarian cancer cells after i.p. injection.³ Of these, the omentum and
121 splenoportal fat are reported to contain analogous milky spots.⁴⁸ We reasoned that a
122 comparison of peritoneal adipose that either contain or lack milky spots could be used to
123 determine the contributions of adipocytes and milky spots to the lodging and progressive
124 growth of ovarian cancer cells in physiologically relevant tissues. *In vivo* studies showed that
125 milky spots are an absolute requirement for cancer cell lodging on peritoneal adipose.
126 Consistent with this finding, conditioned media from milky spot-containing adipose tissue has
127 an enhanced ability to direct cell migration as compared to conditioned media from milky
128 spot-deficient adipose tissue. Studies using a panel of immune-deficient mice showed that
129 the number and size of omental milky spots is not dependent on the mouse genetic
130 background. Similarly, ovarian cancer cell colonization does not depend on the immune
131 composition of the milky spot. Finally, consistent with the role for lipids as an energy source
132 for ovarian cancer cell growth, *in vivo* time-course studies found an inverse relationship
133 between metastatic burden and adipocyte content in the omentum. Our findings support a

134 two-step model wherein both milky spots and adipose have specific roles in colonization of
135 the omentum by ovarian cancer cells.

136 **Materials and Methods**

137 **Cell Lines:** The SKOV3ip.1 human ovarian carcinoma cell line⁴⁹ was a generously supplied
138 by Dr. Gordon Mills (M.D. Anderson Cancer Center, Houston, TX). These cells were
139 maintained in standard growth media [DMEM containing D-glucose (4.5 g/L), L-glutamine
140 (584 mg/L) and sodium pyruvate (110 mg/L) (Mediatech, Manassas, VA), supplemented with
141 5% Fetal Bovine Serum (FBS; Atlanta Biologicals, Lawrenceville, GA), 1%
142 Penicillin/Streptomycin (P/S) solution (5,000 IU/ml Penicillin + 5,000 µg/ml Streptomycin
143 mixture), 1X non-essential amino acids and 2X MEM vitamin solution (all from Mediatech)].
144 The ID8 mouse ovarian carcinoma cell line, derived from and syngeneic to mice of the
145 C57Bl/6 background⁵, was generously provided by Dr. Katherine Roby (University of Kansas
146 Medical Center, Kansas City, KS). These cells were maintained in a standard growth media
147 [DMEM supplemented with 4% FBS, 1% P/S solution and 5 µg/ml insulin-transferrin-sodium
148 selenite (Roche, Indianapolis, IN)]. All cells were maintained under standard tissue culture
149 conditions (i.e. in a humidified incubator at 37°C supplemented with 5% CO₂).

150 **Mice:** All mice were housed and maintained according to Institutional Animal Care and Use
151 guidelines and under the supervision of the University of Chicago Animal Resource Center.
152 Outbred CD1 mice were obtained from Charles River (Wilmington, MA). Inbred B6
153 (C57Bl/6NHsd; immunocompetent), Nude (Athymic Nude-*Foxn1*^{nu}; which are T cell deficient)
154 and BN XID (Hsd:NIHS-*Lyst*^{bg}*Foxn1*^{nu}*Btk*^{xid}; which are NK cell and T cell deficient) mice were
155 obtained from Harlan Laboratories (Indianapolis, IN). Rag1 (B6.129S7-*Rag1*^{tm1Mom}/J; which
156 have no mature T or B cells, no CD3 positive and no T cell receptor α - β positive cells) and

157 Igh6 (B6.129S2-Ighm^{tm1Cgn}/J; which lack mature B cells) mice were obtained from Jackson
158 Laboratories (Bar Harbor, ME).

159 **Harvesting Mouse Tissues:** The locations of the well-defined depots of adipose used for the
160 studies described herein are described.³ Omenta were harvested as described by Khan *et*
161 *al.*⁷ Splenoportal fat bands were collected by isolating the thin, fatty band of tissue connecting
162 the hilum of the spleen to the pancreas,⁴⁸ releasing it from the pancreas and then carefully
163 dissecting it from the spleen. Uterine fat was excised from the uterine horns using dissecting
164 scissors. Similarly, gonadal fat was excised from the ovaries. Mesenteries were collected by
165 first cutting the junction between the small intestine and the pylorus, firmly gripping the free
166 end of the small intestine with forceps, “peeling” the small intestine from the mesentery by
167 pulling the tissue slowly and finally releasing the mesentery from the mesentery root with
168 dissecting scissors.

169 **Preparation of Tissues for Standard Histologic Evaluation:** Tissues were processed for
170 histological evaluation immediately after harvest or *ex vivo* culture. Larger tissues (whole
171 gonadal fat, uterine fat and mesentery) were fixed in 10% neutral buffered formalin (Sigma
172 Aldrich, St. Louis, MO) for 48 hrs at 4°C. Smaller tissues (whole omentum, splenoportal fat
173 and tissue equivalents of uterine fat and mesentery) were fixed overnight (12-16 hrs) in 5%
174 neutral buffered formalin (Sigma Aldrich) at 4°C. Fixed tissue was stored in 70% ethanol at
175 4°C until it was embedded in paraffin. Tissues were sectioned (4 µm) and hematoxylin &
176 eosin (H&E) stained by the University of Chicago Human Tissue Resource Center. All
177 pathological evaluation of tissue was performed by MC under blind conditions.

178 **Immunohistochemistry:** Tissue sections were deparaffinized in xylenes and rehydrated
179 through serial dilutions of ethanol to distilled water. Sections were subsequently incubated in
180 antigen retrieval buffer (DAKO, Carpinteria, CA) and heated in steamer to 97°C for 20 min.

181 Primary antibodies were diluted in Tris Buffered Saline and Tween (TBST) with 0.025% Triton
182 X-100. Pan-cytokeratin (clone: H-240 #sc-15367, Santa Cruz Biotechnology, Santa Cruz, CA)
183 and CD45 (clone: H130 #14-0459-82, eBioscience, San Diego, CA) were applied to tissue
184 sections at a 1:100 dilution and incubated for 1 hr at room temperature. After application of
185 primary antibody, slides were rinsed in Tris-Buffered Saline (TBS) and biotinylated secondary
186 antibody, diluted in TBST with 10% mouse serum (Jackson ImmunoResearch, West Grove,
187 PA) was applied to the slides. For pan-cytokeratin staining, sections were incubated with goat
188 anti-rabbit IgG (1:200 dilution, #BA-1000, Vector Laboratories, Burlingame, CA) for 30 min at
189 room temperature. For CD45 staining, sections were incubated with anti-mouse IgG (1:100
190 dilution, #BA-2001, Vector Laboratories) for 30 min at room temperature. The biotinylated
191 secondary antibody was detected using the Vectastain Elite ABC kit (Vector Laboratories)
192 and DAB (DAKO) peroxidase substrate.

193 **Peritoneal Metastasis Assay:** Exponentially growing SKOV3ip.1 or ID8 cells were
194 trypsinized and prepared as a single cell suspension at a concentration of 2×10^6 cells/ml in
195 cold phosphate buffered saline (PBS). Animals were injected intraperitoneally with 500 μ l of
196 the cell suspension (1×10^6 cells) at a point equidistant between the inguinal papilla. For all
197 experiments, 500 μ l of cold PBS was injected as a negative control in a parallel group of
198 control mice. At the experimental endpoint of each assay, mice were sacrificed via CO₂
199 asphyxiation. Tissues were then harvested, processed, sectioned and stained as described
200 herein.

201 **Preparation of Tissue-Conditioned Media:** Tissues were harvested under sterile conditions
202 and immediately placed in sterile cold PBS. After collection, "tissue equivalents" were
203 prepared by first weighing the omentum from an individual mouse and then excising a strip of
204 uterine fat or branch of mesentery of equivalent weight. In our studies we found that a single

band of splenoportal fat weighs 2.90 ± 0.62 mg (mean \pm 2SD). Given that this is approximately one half the weight of an omentum (6.72 ± 2.82 mg), two fat bands were combined to make one tissue equivalent. Each tissue equivalent was placed in its own well of a polystyrene 12-well plate containing 1.25 ml DMEM/F-12 supplemented with 20% FBS and 1% P/S and incubated at 37°C with 5% CO₂ as described by Khan *et al.*⁷ Tissues were allowed to acclimate to these *ex vivo* conditions for 24 hrs after which the serum-containing media was removed, tissues were carefully rinsed with PBS and then placed in 1.25 ml serum-free DMEM/F-12 (containing 1% P/S). After 24 hrs of conditioning, the serum-free media was collected and used for the transwell migration assays as described. For longer *ex vivo* culture, media was changed to fresh serum-free DMEM/F12 at subsequent 24 hr intervals, such that the tissues were fed for the first 24hrs and starved for the remainder of the assay. Conditioned media from each 24hr interval was collected. In order to ensure that stimulatory activity in the conditioned media was due to secretion of chemotactic factors and not cellular breakdown, tissue integrity was assessed by H&E staining and light microscopy as described by Khan *et al.*⁷ Tissue integrity was further assessed by manually counting the number of healthy and necrotic adipocytes on H&E sections and formulating a percentage of live tissue present. Tissue function was also confirmed by measuring interleukin-6 (IL-6) levels in the conditioned media. IL-6 is produced by adipose, mesothelial cells and immune cells and immediately secreted into the microenvironment.⁵⁰ Specifically, enzyme-linked immunosorbent assays (ELISA) for IL-6 were performed on tissue-conditioned media using a Mouse IL-6 Platinum ELISA kit (eBioscience, San Diego, CA) following the manufacturers instructions.

Transwell Migration Assay: All migration assays used the same physical setup with 1 mL of conditioned or control media (unconditioned culture media) to be tested for chemoattractant

229 activity placed in the lower chamber and cancer cells placed in 8 μ m-pore PET membrane
230 transwell (BD Falcon, Franklin Lakes, NJ) which served as the upper chamber of the assay
231 apparatus. Exponentially growing SKOV3ip.1 or ID8 cells were trypsinized and resuspended
232 in serum-free DMEM at a concentration of 3.33×10^5 cells/ml or 2.50×10^5 cells/ml,
233 respectively. In each case, 600 μ l of cell suspensions (SKOV3ip.1 = 2.0×10^5 total; ID8 = 1.5
234 $\times 10^5$ total) were added to the transwells. Cells were allowed to migrate in response to signals
235 from conditioned or control media for 6 hrs under standard tissue culture conditions.

236 After incubation, media was aspirated from both chambers and the upper and lower
237 surfaces of the membrane were washed once with cold PBS. The membrane was fixed in
238 10% buffered formalin for 10 min at room temperature. Residual formalin was removed by
239 washing with cold PBS. Both sides of the membrane were subsequently stained with a 0.05%
240 crystal violet solution (Fisher, Fair Lawn, NJ) for 30 min at room temperature and washed
241 once with tap water. Cells that had not migrated through the membrane were removed by
242 gently wiping the upper membrane surface with a cotton swab and the membrane was
243 allowed to air-dry overnight. Finally, the membrane was removed from the transwell scaffold
244 using a scalpel and mounted top-surface-facing-up onto a slide using Permount as the
245 mounting medium (Fisher). The number of cells that had migrated through the membrane
246 was quantified by taking 5 random images per slide at 100x with an Axiovert 200M inverted
247 microscope (University of Chicago Integrated Microscopy Core Facility). ImageJ (NIH) was
248 used to quantitate the total number of migrated cells present in each image. The counts from
249 each of the five images were totaled to give the number of migrated cells for each sample. n=
250 5 for all conditions.

251 **Milky Spot Identification Using Carbon Nanopowder Uptake:** Carbon nanopowder was
252 used to stain milky spot phagocytes similarly to described methods.³¹ Briefly, carbon (<50 nm

253 particle size; Sigma Aldrich, St. Louis, MO) was mixed with PBS at a concentration of 5
254 mg/ml and sonicated for 20 min to create a homogenous suspension. The suspension was
255 autoclaved, allowed to cool to room temperature and re-sonicated for 20 min immediately
256 before injection. Mice were i.p. injected with 800 μ l of the carbon suspension. At 14 days post
257 injection (dpi) mice were euthanized. Omenta were harvested and fixed in 10% formalin for 2
258 hrs at room temperature. Whole fixed tissue was dehydrated through increasing
259 concentrations of ethanol (i.e. 70%, 90% and 2x 100%; 10 min each) and cleared in xylenes
260 for 10 min. Finally, tissues were whole-mounted between a slide and coverslip using
261 Permount. Images of the whole-mounted tissues were captured using a CRi Pannoramic
262 Scan Whole Slide Scanner in the University of Chicago Light Microscopy Core Facility and
263 images were processed with Pannoramic Viewer software (3D Hitech, Budapest, Hungary).

264 **Milky Spot Identification Using Giemsa Staining:** Excised omenta were prepared for
265 standard histologic evaluation, with careful orientation of the tissues while paraffin embedding
266 to produce longitudinal sections. The whole omentum was serially sectioned (4 μ m) and
267 every third section was Giemsa stained (Fluka, St. Louis, MO). Slides were deparaffinized in
268 xylenes and rehydrated through serial dilutions of ethanol to water. Slides were stained in 5%
269 Giemsa solution (prepared in tap water) for 4 min, rinsed in tap water for 60 sec, allowed to
270 air-dry and coverslipped using Permount. Images of the stained slides were captured using a
271 CRi Pannoramic Scan Whole Slide Scanner in the University of Chicago Light Microscopy
272 Core Facility and images were processed with Pannoramic Viewer software (3D Hitech,
273 Budapest, Hungary).

274 **Three-Dimensional Rendering of Giemsa-Stained Omentum:** ImageJ software was used
275 to render a three-dimensional image of a B6 omentum. Imaged, Giemsa-stained omentum
276 sections from an entire omentum were aligned using the StackReg plugin.⁵¹ The resulting

277 stack was Inverted and the 3D Project tool, with the interpolate function set to a slide spacing
278 of 4 μm , was used to render a three-dimensional image. This was converted to 8-bit
279 grayscale and false-colored using the Unionjack color scheme.

280 **Milky Spot Identification and Quantitation in Giemsa-Stained Omenta:** ImageJ software
281 was used to quantify the milky spot volume in the Giemsa-stained omental sections. Images
282 were converted to 8-bit grayscale and Inverted. The Color Balance was adjusted to increase
283 the contrast between the milky spots and surrounding tissue. The image was converted to
284 Binary to reduce background and Inverted again. The Threshold was set using the Auto
285 function, resulting in an image where milky spots are pure black and the rest of the tissue is
286 pure white. The resulting immune aggregates were measured using the Analyze Particles
287 function. This was repeated for each of the Giemsa-stained sections per omentum. Milky spot
288 areas for each omentum section were multiplied by 4 μm and summed to produce a total
289 milky spot volume. The whole omentum volume was measured by adjusting the
290 Brightness/Contrast of a grayscale image to darken the immune aggregates. The Threshold
291 was set to include the entire tissue and the image was converted to a pure black Mask. To
292 create a cohesive border for the omentum, the Find Edges tool was applied and the image
293 was again converted to a Mask and Fill Holes was selected. Again, the omentum was
294 quantified using the Analyze Particle function. Particles smaller than 25 pixels were excluded
295 in the analysis to reduce any background noise. Areas for each omentum were multiplied by
296 4 μm and summed to produce a total whole omentum volume. Macros of the above image
297 processing steps are available as Supplemental Methods. n=5 omenta per each mouse
298 strain.

299 **Quantitation of Adipocyte Area in Omenta Over the Timecourse of Metastatic**
300 **Colonization.** Omenta were harvested from mice at 1, 3, 6 and 9 weeks after cancer cell

301 injection and tissues were prepared for standard histologic evaluation. H&E-stained sections
302 were imaged using a CRi Panoramic Scan Whole Slide Scanner. Using ImageJ, section
303 images were converted to 8-bit grayscale, the Brightness/Contrast was adjusted to darken
304 the non-adipocyte tissue and the image Threshold was set (using the Auto function) such that
305 only non-adipocyte structures were transformed to pure black. These structures were
306 measured using the Analyze Particles function with particles smaller than 25 pixels excluded.
307 Resulting areas were summed to produce a total non-adipocyte area. The whole omentum
308 was measured by adjusting the Threshold of a Brightness/Contrast-adjusted grayscale image
309 such that the whole area is converted to pure black. Again, the omentum was quantified
310 using the Analyze Particle function excluding particles smaller than 25 pixels with the Include
311 Holes option selected. Resulting areas were summed to produce a total omentum area. The
312 percentage of adipocytes was calculated by subtracting the total non-adipocyte area from the
313 total omentum area and dividing that by the total omentum area. Macros of the above image
314 processing steps are available as Supplemental Methods. A total of three sections were
315 quantified per mouse with n=5 mice per timepoint.

316 **Statistics:** All statistical analyses were performed using GraphPad Prism (GraphPad
317 Software, La Jolla, CA). Data was presented as mean of biologic replicates. All error bars
318 represent statistical error of the mean. Statistical significance was determined using one-way
319 analysis of variance (ANOVA) followed by Tukey-Kramer multiple comparison tests. One, two
320 and three asterisks represent $p<0.05$, $p<0.01$, $p<0.001$, respectively.

321 **Results**

322 **Several sources of adipose tissue are accessible to ovarian cancer cells in the**
323 **peritoneal cavity.** The organ-specificity of ovarian cancer metastasis is often explained by
324 the omentum's anatomic location and tissue composition.^{6,46} However, to our knowledge,

325 these assertions have not been tested *in vivo* by evaluating ovarian cancer cell lodging or
326 growth in other adipose depots that are accessible during peritoneal dissemination. There are
327 five major adipose-rich structures in the peritoneal cavity.³ As shown in Figure 1A, a lateral
328 view of a ventral dissection allows visualization of the omentum (OM), gonadal fat (GF),
329 uterine fat (UF) and mesentery (MY). The ovary (ov), uterine horn (uh) and small intestine (si)
330 are indicated as points of reference. Further dissection allows for clear visualization of the
331 splenoportal fat (SP), which connects the hilum of the spleen to the pancreas (Figure 1B),
332 and the omentum, shown isolated from the pancreas (Figure 1C). The gross structure and
333 relative size of these tissues is shown in Figure 1D. Interestingly, it has been reported that
334 the splenoportal fat contains milky spots that are analogous to omental milky spots in both
335 composition and structure.⁴⁸ In agreement with these published findings, histologic evaluation
336 of tissues confirmed the presence milky spots in the omentum and splenoportal fat and the
337 absence of milky spots in uterine and gonadal fat (Supplemental Figure S1). In the case of
338 the mesentery, our findings differed somewhat from the literature⁵² as we only observed
339 occasional minute clusters of lymphoid cells which were smaller and less structurally distinct
340 than the milky spots seen in omental and splenoportal fat (Supplemental Figure S1). Taken
341 together these data show that during peritoneal dissemination, ovarian cancer cells have
342 access to and can interact with adipose tissues that either contain or lack milky spot
343 structures.

344 **Ovarian cancer cells only colonize peritoneal adipose that contains milky spots.** As
345 described in the introduction, a review of the literature showed that ovarian cancer's
346 predilection for omental metastasis formation can be ascribed to either adipose-driven or
347 milky spot-driven mechanisms. However, these models were prompted by reductionist
348 studies focusing on either structural features (i.e. milky spots) or cellular components (i.e.

adipocytes) of omental tissue.^{30,44,47} The availability of peritoneal fat depots that contain or lack milky spot structures enabled us to experimentally distinguish between the two models in the physiologically relevant setting of the peritoneal cavity. We reasoned that if colonization were purely adipocyte-driven, ovarian cancer cells would colonize all of the peritoneal adipose depots after i.p. injection. In contrast, if milky spots were required for this process, only the omentum and splenoportal fat would be colonized. To test this, we assessed the lodging and growth of ID8 cancer cells on the five distinct peritoneal fat depots after i.p. injection into B6 mice. At 7 days post-injection (dpi), large colonies of ID8 cells were only seen within the milky spots of both the omentum and splenoportal fat (Figure 2A, left). No ovarian cancer cells were detected in the uterine or gonadal fat (Figure 2A, right). When the mesentery was examined, the rare lodged cancer cells seen were associated with the few immune aggregates present in that tissue (data not shown). Even at an assay endpoint (42 dpi) when animals have peritoneal disease burden that requires euthanasia, no ovarian cancer cells could be detected by histologic evaluation of the fatty tissues lacking milky spots (data not shown). As a confirmation of these findings, human SKOV3ip.1 cells were similarly injected into Nude mice. At 7 dpi large colonies of SKOV3ip.1 cells were observed in milky spots within the omentum and splenoportal fat (Figure 2B). Using IHC for human pan-cytokeratin, we confirmed that these lesions were composed of epithelial (SKOV3ip.1) cells intermingled with the immune cells. The specificity of staining was confirmed using an IgG control for the pan-cytokeratin antibody (Figure 2B).

Omental tissues secrete a factor(s) that can promote ovarian cancer cell migration. Ovarian cancer cells specifically localize to the omentum within minutes after i.p. injection.^{4,7,42} This suggests that omental tissue produces a factor(s) that promotes cancer cell homing; however, previous studies have only examined the contribution of isolated

373 adipocytes.⁴⁷ To address this gap in knowledge, we first tested the ability of omentum-
374 conditioned media to promote directed cancer cell migration. Using a modification of our
375 published method for *ex vivo* organ culture,⁷ omenta were excised and allowed to normalize
376 in DMEM/F12 media containing 20% FCS for 24 hrs. Tissues were then rinsed with PBS,
377 placed in serum-free DMEM/F12 and maintained for up to 5 days *ex vivo*. Tissue integrity
378 was assessed both histologically by visually evaluating intact (round, continuous cell
379 membrane) versus necrotic (stellate, discontinuous cell membrane) adipocytes and
380 functionally by measuring the level of IL-6 in the conditioned media every 24 hrs. In
381 agreement with our previously published studies,⁷ omental tissues did not show loss of
382 integrity or function under these conditions (Supplemental Figure S2, top row).

383 The experimental design used for the migration assays is summarized in Figure 3A. After
384 normalization in DMEM/F12 containing 20% FCS, omenta were rinsed with PBS and allowed
385 to condition serum-free DMEM/F12 for 24 hrs (subsequently referred to as conditioned
386 serum-free media; CSF). Omenta maintained in serum-free (SF) media are termed starved
387 omenta (SOM). The combinations of omenta and media used as chemoattractants for the 6
388 hr migration assay are summarized in Figure 3B, upper panel, while representative
389 membranes from the migration assays are shown in Figure 3B, lower panel. The number of
390 cells that migrated to the lower side of the membrane was determined by summing the
391 number of cells in each of 5 independent fields observed at 100x magnification.

392 Initial studies tested the ability of omenta harvested from CD1 mice to promote migration of
393 both mouse ID8 and human SKOV3ip.1 cells (Figure 3C). With both cell types, the
394 combination of SF media and SOM during the 6hr migration assay caused small, yet
395 reproducible, stimulation of migration above that seen in the SF media controls. In contrast,
396 CSF media served as a strong chemoattractant for both ID8 and SKOV3ip.1 cells, resulting in

397 a greater than 150-fold increase in migration relative to SF media controls. The addition of
398 SOM to the CSF media (CSF+SOM) did not further enhance cell migration. To ensure that
399 these results are not specific to omenta harvested from CD1 mice, CSF from B6 and Nude
400 mice were also tested in their ability to promote ID8 and SKOV3ip.1 cell migration. As shown
401 in Figure 3D, migration of ID8 and SKOV3ip.1 cells were statistically identical in response to
402 conditioned media from both B6 and Nude omenta. Interestingly, ID8 cells show a
403 consistently higher level of migration than SKOV3ip.1 cells in response to media conditioned
404 by CD1, B6 and Nude mice. Taken together, these experiments showed that intact omental
405 tissue can be used as a starting point for efforts to identify the secreted factor(s) that promote
406 ovarian cancer cell homing to omental tissues.

407 **Milky spot-containing tissues show enhanced ability to stimulate directed migration.**

408 In their work, Nieman *et al.* showed that adipocytes cultured *in vitro* secreted cytokines that
409 can promote migration of SKOV3ip.1 ovarian cancer cells.⁴⁷ This raised the possibility that
410 migration of cancer cells toward omentum-conditioned media could be a strictly adipose-
411 driven process. If that were the case, we predicted that media conditioned by adipose tissue
412 lacking milky spots would promote migration of ovarian cancer cells to the same extent as
413 milky spot-containing adipose tissue. Alternatively, if milky spots are responsible for organ-
414 specific homing, we expected that conditioned media from tissues containing milky spots
415 could have an enhanced ability to promote migration. To distinguish between these
416 possibilities, CSF media was prepared using weight-matched tissue equivalents of omentum,
417 splenoportal fat, uterine fat and mesentery and used as a chemoattractant in transwell
418 migration assays. As shown in Supplemental Figure S2, tissues did not show loss of integrity
419 or function for the duration of the migration assay. However, it was noted that the IL-6
420 production of the cultured uterine fat dropped significantly at 3 days in culture (Supplemental

421 Figure S2). The migration-promoting activity of CSF prepared from each of these tissues is
422 summarized in Figure 3E. Media conditioned by omenta and splenoportal fat caused a 95-
423 fold increase in cell migration as compared to SF media controls. In contrast, the absence of
424 milky spots in uterine fat and mesentery corresponded with 75% reduction in the migration-
425 stimulatory activity in their conditioned media (Figure 3E). Taken together, these functional
426 studies bridge the adipocyte-driven and milky spot-driven models and argue that the
427 presence of milky spots increases the chemoattractive potential of peritoneal fat depots.

428 **The number and size of omental milky spots is not dependent on the mouse genetic**
429 **background.** Immune cells, including macrophages, lymphocytes and mast cells, are integral
430 to both the composition and function of omental milky spots.^{31,36,39,41} This raised the question,
431 “Are specific immune cell types required for milky spot formation, maintenance and function?”
432 As a first step toward answering this question, we tested the possibility that mutations
433 depleting or inactivating specific lymphocyte populations (i.e. immunodeficient mouse
434 models) could affect the number and size of omental milky spots. The majority of published
435 studies use two standard methods to identify milky spots. The first employs a nonspecific
436 esterase stain, which colors macrophages and T-lymphocytes dark red.³¹ In our hands, this
437 method yielded highly variable results that were not of sufficient quality or resolution for
438 quantitative analyses (data not shown). A second method employs i.p. injection of a carbon
439 nanopowder suspension, which is phagocytosed by peritoneal macrophages over a period of
440 days.³¹ Tissues are subsequently harvested, whole-mounted and the number and/or area of
441 the black-staining macrophages are used as a measure of milky spot number and size. When
442 this method works correctly the milky spot structures are crisp and well defined, and they can
443 be visualized and counted under light microscopy (Figure 4A). However, we found that this
444 technique can give inconsistent results because carbon plaques (indicated by arrows) often

445 form on various peritoneal surfaces (Figure 4B). This plaque formation prevents both precise
446 isolation (excision) of the omentum and accurate evaluation of milky spot area in the whole-
447 mounted tissue.

448 To circumvent this problem, we developed a novel technique to visualize the milky spots
449 on a whole-mount scale using Giemsa staining. In this approach, excised omenta were
450 paraffin-embedded and the entire organ serially sectioned at 4 μ m (resulting in ~30-60
451 sections). Every third section was stained in a 5% Giemsa solution and images of the stained
452 tissues captured using a CRi Panoramic Scan Whole Slide Scanner (Figure 4C). As shown
453 in Figure 4D, milky spots appear as dark blue-staining areas. The identity of these regions as
454 milky spots was confirmed in serial sections by both H&E staining and IHC for CD45+
455 (Cluster of Differentiation 45; common lymphocyte marker) cells (Figures 4E and 4F,
456 respectively). Milky spots from B6, Nude, Rag1, Igh6 and BN XID mice were successfully
457 stained with Giemsa using this method (Supplemental Figure S3). By stacking and aligning
458 all of the Giemsa stained images from one omentum, we were able to produce a three-
459 dimensional rendering of a mouse omentum that accurately depicts the tissue architecture
460 and presents a novel view of the location and structure of milky spots (Supplemental Video
461 S4).

462 We used ImageJ to process the Giemsa-stained omentum slices in order to produce
463 images that display both milky spots (Figure 4G) and the whole omentum area (Figure 4H) as
464 pure black pixels (the processing steps are detailed in the Materials and Methods section).
465 These black pixels were quantified using the Analyze Particle feature of ImageJ producing a
466 milky spot area and a whole omentum area for each slice. Since each section was cut at 4
467 μ m, those areas were summed and multiplied by 4 μ m to produce milky spot and total volume
468 for each omentum. Surprisingly, we found no difference among the milky spot volumes

469 (Figure 5A) or the omentum volumes (Figure 5B) for the 5 mouse strains. Furthermore, no
470 significant difference was found when the milky spot volume was expressed as a percentage
471 of the total omentum area (Figure 5C). These data show that the volume of milky spots
472 present in the omentum is not affected by deficiency or absence of T cells, B cells or NK cells
473 in these well-established immune-competent and immunodeficient mouse strains.

474 ***In vivo* colonization of omental milky spots by ovarian cancer cells is not dependent**
475 **on their immune cell composition.** As a first step toward understanding the effect of the
476 immune cell composition of milky spot structures on ovarian cancer cell colonization,
477 experimental metastasis assays were conducted using our panel of immune competent and
478 deficient mice. Specifically, 1×10^6 ID8 ovarian cancer cells were injected i.p. into syngeneic
479 B6 mice. In parallel, 1×10^6 SKOV3ip.1 human ovarian cancer cells were injected into Nude,
480 Rag1 and BN XID mice. Cancer cell foci were observed within milky spots in each of these
481 mouse strains at 7 dpi (Figure 6A). To confirm that the infiltrating cells were in fact
482 SKOV3ip.1, we stained relevant sections for epithelial pan-cytokeratin. SKOV3ip.1 lesions
483 were cytokeratin-positive (Figure 6B) with no discernable background staining in the IgG
484 control for the pan-cytokeratin antibody or PBS-injected control mice. Thus, ovarian cancer
485 cell colonization of omental milky spots is not affected by deficiency or absence of T cells, B
486 cells or NK cells in these mouse strains.

487 **During progressive growth ovarian cancer cells replace omental adipose.**
488 Mechanistic studies by Nieman *et al.* indicated that ovarian cancer cells could use adipocytes
489 as an energy source for tumor growth.⁴⁷ If this holds true *in vivo*, we predicted that as cancer
490 cells proliferate, they interact with and consume adipocyte lipids. The ultimate outcome of this
491 inverse relationship between cancer cell area and adipocyte area would be that, at the
492 experimental endpoint, the omental adipose would be replaced completely with cancerous

493 tissue. To test this notion, 1×10^6 ID8 ovarian cancer cells were injected i.p. into a cohort of
494 B6 mice. Groups of 5 mice were euthanized and tissues collected for histologic analysis at 1,
495 3, 6 and 9 weeks post injection (Figure 7A). Consistent with an inverse relationship between
496 ovarian cancer cell growth and adipocyte depletion, there is a marked reduction in the
497 adipocyte area over time. To quantify this change, we used an image processing protocol
498 similar to milky spot quantification (detailed in the Materials and Methods) to produce images
499 that show all non-adipocyte areas as pure black pixels as well as the total omentum area as
500 pure black pixels. Those pixels were quantitated in three separate sections per mouse and
501 showed a linear decrease in the percentage of adipocytes in the omentum corresponded to
502 the expansion of ID8 cancer cell lesions (Figure 7B). These data are consistent with cancer
503 cells' utilization of lipids stored in adipocytes as an energy source for their continued growth.

504 **Discussion**

505 There is now considerable literature on the structure and function of milky spots in both the
506 omentum and extraomental sites. Beginning in the 1970s, investigators noted that ascites
507 tumors had a proclivity for these structures.⁴³ Subsequent studies confirmed and refined
508 these findings.^{4,7,42} The strength of this work is that it implies a functional role for milky spots
509 in the early steps of omental colonization. However, the weakness of the “milky spot-driven”
510 model prompted by this body of literature is that the studies on which it is based do not
511 consider the potential contribution(s) of adipocytes and other cells within the adipose-rich
512 region. While the failure to consider the contribution of omental adipose in cancer metastasis
513 is consistent with the now-antiquated view of fat as an inert component of connective
514 tissues,^{16,21,22} it is a fundamental oversight that must be addressed if we are to understand
515 the organ specificity of ovarian cancer cells.

516 In contrast, the adipocyte-driven model prompted by the findings of Nieman *et al.*, showed
517 that in omental metastases, ovarian cancer cells at the interface with adipocytes contained
518 abundant lipids.⁴⁷ *In vitro* studies showed that the adipocytes transfer lipid droplets that
519 contain fatty acids that can be used as an energy source to ovarian cancer cells.⁴⁷ The
520 strength of their studies is that they focused on human ovarian cancers and identified a novel
521 function for adipocytes in the progressive growth of ovarian cancer lesions. The weakness of
522 this work lays in its effort to show that adipocytes drive, and are solely responsible for, early
523 steps in omental colonization. The case for adipose as the sole determinant of the ovarian
524 cancer's organotropic metastasis was based on an incomplete examination of the literature
525 and a biased approach to experimental design. As a result of the focus on adipocytes,
526 important clues in the data were overlooked and the potential contributions of milky spots,
527 vasculature or other unique characteristics of the omentum were neither tested nor
528 discussed. Thus, like the milky spot-driven model, this model is also limited by the
529 reductionist studies upon which it was based.

530 Despite their strengths, neither the milky spot-driven nor the adipocyte-driven models
531 address the intimate and dynamic interactions among milky spot structures, adipocytes and
532 other components of the adipose-rich areas. Studies herein bridge and organize findings from
533 both the milky spot- and adipocyte-driven models into a coherent model of omental
534 colonization. Our data show that gonadal fat, uterine fat and mesentery secrete a factor(s)
535 that promotes directed migration; however, results from *in vivo* assays show that ovarian
536 cancer cells do not colonize these tissues. This suggests that colonization requires additional
537 chemotactic signals and/or tissue structures. In support of this notion, *in vivo* assays showed
538 that ovarian cancer cells efficiently colonize milky spots in the splenoportal fat (Figure 2). In
539 addition, media conditioned by adipose containing milky spot structures showed significant

enhancement in its ability to promote directed cancer migration. After lodging within milky spot structures, ovarian cancer cells begin to proliferate. Finally, the role of adipocytes in supplying energy for cancer cells' growth is supported by the direct relationship between cancer cell growth and adipocyte depletion. These agree with breast cancer models where cancer growth causes a reduction in adipocyte number and size (reducing the adipocyte-to-cancer area ratio), implying lipolysis and possible adipocyte de-differentiation.⁵³

Our finding that milky spots are required for colonization of peritoneal adipose confirms and extends previous work^{4,7,26,30,42-46} and provides a foundation for studies to identify milky spot components involved in cancer cell homing and invasion. As a first step toward this goal, the use of immunodeficient mouse strains allowed us rule out a requirement for B cells, T cells or NK cells for ovarian cancer cell lodging within milky spots, confirming and expanding on the findings of Lotan *et al.*⁹ Previous studies have shown that mast cells and macrophages are frequently observed in the milky spots.^{32,35,36,38} Macrophages are an intriguing candidate as they can initiate the directed migration of disseminated mammary cells using secreted epidermal growth factor (EGF)⁵⁴ and have been shown to assist the survival and growth of established tumors.⁵⁵⁻⁵⁷ Further, the depletion of peritoneal macrophages has been shown to decrease ovarian cancer tumor burden on the diaphragm at the experimental endpoint.⁵⁸ Altogether, milky spot macrophages are potentially the source of the omentum's chemotactic properties and warrant future study.

Both the mesothelium and vasculature of milky spots may also contribute to milky spot colonization. A majority of studies support the notion that cancer cells exploit the stomata over the milky spots to gain access to the interior milky spot structures.^{46,59} It is unclear whether the cancer cells simply push their way through the stomata during milky spot invasion⁶⁰ or if the mesothelial cells surrounding the stomata actively assist in the localization

564 process by secreting a chemotactic factor.^{30,44} Similarly, endothelial cells within the highly
565 fenestrated capillaries of the omental glomeruli may play a role in promoting cancer cell
566 migration to and subsequent growth within milky spot structures. For example, previous
567 studies have shown that VEGF-A produced by endothelial cells promotes the directed
568 migration of breast cancer cell.⁶¹ Furthermore, endothelial cells can secrete IL-6, CXCL8 and
569 EGF to stimulate migration and anoikis resistance of head and neck squamous cell
570 carcinoma.⁶² In fact, the dense capillary network may promote cancer progression in that high
571 tumor microvessel density can negatively predict ovarian cancer survival.⁶³ Taken together,
572 these attributes also make endothelial cells excellent candidates as primary promoters of
573 metastatic tumor growth at the omentum.

574 While we found that milky spot structures are necessary for colonization, the literature
575 indicates that they may not be sufficient for colonization. Studies indicate that these
576 structures are also present in other serous membranes including the pleural mesothelium, a
577 site where we do not observe ovarian cancer cells in *in vivo* assays.^{26,48,64} This suggests that
578 in addition to providing energy, adipocytes influence milky spot function. It is now well
579 established that lipid droplets, such as those transferred to ovarian cancer cells,⁴⁷ are in fact
580 highly-regulated organelles that can participate in cell activation and metabolism. The
581 potential contribution(s) of lipid droplets to inflammatory and neoplastic processes is a subject
582 of intense interest.⁶⁵ Of particular relevance to omental colonization, reports suggest that
583 adipocytes and lymphoid cells interact in a paracrine manner giving the adipocytes properties
584 that distinguish them from classical adipocytes.^{26,66,67} Similarly, association with cancer cells
585 results in dysfunctional adipocytes that overexpress adipokines and proteases that aid in
586 tumor progression and colonization. For example, adipokines such as IL-6 and IL-8 may
587 function as general chemoattractants that work in concert with additional factors that specify

588 milky spot localization.^{47,53,68} Conversely, cancer cells primed by adipocytes can also show
589 increased migration and invasive potential.^{53,69} For example, breast cancer cells treated with
590 adipocyte-conditioned media showed increased expression of immune cell-related genes,⁷⁰
591 potentially contributing to the milieu of pro-inflammatory cytokines.

592 The growing emphasis on the role of the host tissue microenvironment in metastasis
593 formation stems from the seminal work of Stephen Paget showing that certain tumor cells
594 (the “seed”) have a proclivity for specific organ microenvironment(s) (the “soil”).⁷¹⁻⁷³ A
595 powerful, but often underappreciated, aspect of studies by Paget and other pioneers of
596 metastasis research was their innate appreciation of the unique tissue architecture,
597 physiology and function of the target organ that is essential to understanding metastatic
598 organ specificity.⁷⁴⁻⁷⁷ The studies presented herein integrate milky spot and adipocyte
599 function in the context of the adipose-rich tissues of the omentum. We propose an integrated,
600 two-step model for omental colonization wherein the localization of disseminated cancer cells
601 is dependant upon milky spots. Adipocytes are subsequently required for progressive growth.
602 This model is likely a more accurate representation of the overall process of metastatic
603 colonization. It is our hope that both our findings and discussion of the larger literature will
604 serve as a framework for studies that will continue to refine our understanding of omental
605 colonization. Ultimately, it is our goal to use this information to extend the duration of
606 metastatic suppression.

607 **Acknowledgements**

608 We thank Mr. Nathan Stadick for his critical review of the literature, which contributed to the
609 scholarship of the manuscript. We also thank Dr. Erin Howe for her review and comments,
610 which greatly enhanced the discussion of our results. We are indebted to Ms. Shirley Bond
611 and Dr. Christine Labno, Technical Directors of the integrated microscopy core facility, for

612 their assistance and expertise in the capturing and quantification of the omentum images. We
613 also thank Ms. Terri Lee and Ms. Christy Schmehl of the Human Tissue Resource Center for
614 sectioning and staining of tissue samples.

615

616 **References**

- 617 1. Howlander N, Noone AM, Krapcho M, Neyman N, Aminou R, Waldron W, Altekruse
618 SF, Kosary CL, Ruhl J, Tatalovich Z, Cho H, Mariotto A, Eisner MP, Lewis DR, Chen
619 HS, Feuer EJ, Cronin KA, editors: SEER Cancer Statistics Review, 1973–2009
620 (Vinatage 2009 Populations) [Internet]. Bethesda, MD, National Cancer Institute, 2012
621 Apr. Available from: http://seer.cancer.gov/csr/1975_2009_pops09/
- 622 2. Naora H, Montell DJ: Ovarian Cancer Metastasis: Integrating insights from disparate
623 model organisms. *Nat Rev Cancer* 2005, 5:355–366.
- 624 3. Cinti S: The Adipose Organ. Fantuzzi G, mazzone T, editors. *Adipose Tissue and*
625 *Adipokines in Health and Disease*, Totowa, New Jersey, Humana Press, 2007, pp. 3–
626 19.
- 627 4. Hagiwara A, Takahashi T, Sawai K, Taniguchi H, Shimotsuma M, Okano S, Sakakura
628 C, Tsujimoto H, Osaki K, Sasaki S: Milky spots as the implantation site for malignant
629 cells in peritoneal dissemination in mice. *Cancer Research*, AACR, 1993, 53:687.
- 630 5. Roby KF, Taylor CC, Sweetwood JP, Cheng Y, Pace JL, Tawfik O, Persons DL, Smith
631 PG, Terranova PF: Development of a syngeneic mouse model for events related to
632 ovarian cancer. *Carcinogenesis* 2000, 21:585–591.
- 633 6. Lengyel E: Ovarian Cancer Development and Metastasis. *The American Journal of*
634 *Pathology*, American Society for Investigative Pathology, 2010, 177:1053–1064.
- 635 7. Khan SM, Funk HM, Thiolloy S, Lotan TL, Hickson J, Prins GS, Drew AF, Rinker-
636 Schaeffer CW: In vitro metastatic colonization of human ovarian cancer cells to the
637 omentum. *Clin Exp Metastasis* 2010, 27:185–196.
- 638 8. Kenny HA, Krausz T, Yamada SD, Lengyel E: Use of a novel 3D culture model to
639 elucidate the role of mesothelial cells, fibroblasts and extra-cellular matrices on

- 640 adhesion and invasion of ovarian cancer cells to the omentum. *Int J Cancer* 2007,
641 121:1463–1472.
- 642 9. Lotan T, Hickson J, Souris J, Huo D, Taylor J, Li T, Otto K, Yamada SD, Macleod K,
643 Rinker-Schaeffer CW: c-Jun NH2-terminal kinase activating kinase 1/mitogen-activated
644 protein kinase kinase 4-mediated inhibition of SKOV3ip.1 ovarian cancer metastasis
645 involves growth arrest and p21 up-regulation. *Cancer Research* 2008, 68:2166–2175.
- 646 10. Liebermann-Meffert D: The greater omentum. *Anatomy, embryology, and surgical*
647 *applications*. *Surg Clin North Am* 2000, 80:275–93–xii.
- 648 11. Collins D, Hogan AM, O'Shea D, Winter DC: The omentum: anatomical, metabolic, and
649 surgical aspects. *J Gastrointest Surg* 2009, 13:1138–1146.
- 650 12. Platell C, Cooper D, Papadimitriou JM, Hall JC: The omentum. *World J Gastroenterol*
651 2000, 6:169–176.
- 652 13. Goldsmith HS: *The Omentum: Basic Research and Clinical Application*. 1st ed.
653 Goldsmith HS, editor. New York, Cine Med, Inc, 1990.
- 654 14. Fedorko ME, Hirsch JG: Studies on transport of macromolecules and small particles
655 across mesothelial cells of the mouse omentum. I. Morphologic aspects. *Exp Cell Res*
656 1971, 69:113–127.
- 657 15. Wilkosz S, Ireland G, Khwaja N, Walker M, Butt R, Giorgio-Miller A, Herrick SE: A
658 comparative study of the structure of human and murine greater omentum. *Anat*
659 *Embryol* 2005, 209:251–261.
- 660 16. Wozniak SE, Gee LL, Wachtel MS, Frezza EE: Adipose Tissue: The New Endocrine
661 Organ? A Review Article. *Dig Dis Sci* 2008, 54:1847–1856.
- 662 17. Trayhurn P, Beattie JH: Physiological role of adipose tissue: white adipose tissue as an
663 endocrine and secretory organ. *Proc Nutr Soc* 2001, 60:329–339.
- 664 18. Hauner H: The new concept of adipose tissue function. *Physiol Behav* 2004, 83:653–

- 665 658.
- 666 19. Scherer PE: Adipose tissue: from lipid storage compartment to endocrine organ.
667 Diabetes 2006, 55:1537–1545.
- 668 20. Kershaw EE, Flier JS: Adipose tissue as an endocrine organ. J Clin Endocrinol Metab
669 2004, 89:2548–2556.
- 670 21. Wang P, Mariman E, Renes J, Keijer J: The secretory function of adipocytes in the
671 physiology of white adipose tissue. J Cell Physiol 2008, 216:3–13.
- 672 22. Conde J, Scotece M, Gómez R, López V, Gómez-Reino JJ, Lago F, Gualillo O:
673 Adipokines: biofactors from white adipose tissue. A complex hub among inflammation,
674 metabolism, and immunity. Biofactors 2011, 37:413–420.
- 675 23. Frühbeck G, Gómez-Ambrosi J, Muruzábal FJ, Burrell MA: The adipocyte: a model for
676 integration of endocrine and metabolic signaling in energy metabolism regulation. Am J
677 Physiol Endocrinol Metab 2001, 280:E827–E847.
- 678 24. Tilg H, Moschen AR: Adipocytokines: mediators linking adipose tissue, inflammation
679 and immunity. Nat Rev Immunol 2006, 6:772–783.
- 680 25. Rajala MW, Scherer PE: Minireview: The adipocyte--at the crossroads of energy
681 homeostasis, inflammation, and atherosclerosis. Endocrinology 2003, 144:3765–3773.
- 682 26. Michailova KN, Usunoff KG: The milky spots of the peritoneum and pleura: structure,
683 development and pathology. Biomedical Reviews, Varna, Bulgaria, 2004, 15:47–66.
- 684 27. Simer P: On the morphology of the omentum, with especial reference to its lymphatics.
685 American Journal of Anatomy, Wiley Subscription Services, Inc., A Wiley Company,
686 1934, 54:203–228.
- 687 28. Ackermann PC, De Wet PD, Loots GP: Microcirculation of the rat omentum studied by
688 means of corrosion casts. Acta Anat (Basel) 1991, 140:146–149.
- 689 29. Shimotsuma M, Shields J, Simpson-Morgan M, Sakuyama A, Shirasu M, Hagiwara A,

- 690 Takahashi T: Morpho-physiological function and role of omental milky spots as
691 omentum-associated lymphoid tissue (OALT) in the peritoneal cavity. *Lymphology*
692 1993, 26:90.
- 693 30. Gerber SA, Rybalko VY, Bigelow CE, Lugade AA, Foster TH, Frelinger JG, Lord EM:
694 Preferential Attachment of Peritoneal Tumor Metastases to Omental Immune
695 Aggregates and Possible Role of a Unique Vascular Microenvironment in Metastatic
696 Survival and Growth. *The American Journal of Pathology*, American Society for
697 Investigative Pathology, 2006, 169:1739–1752.
- 698 31. Shimotsuma M, Kawata M, Hagiwara A, Takahashi T: Milky spots in the human greater
699 omentum. Macroscopic and histological identification. *Acta Anat (Basel)* 1989,
700 136:211–216.
- 701 32. Shimotsuma M, Simpson-Morgan MW, Takahashi T, Hagiwara A: Activation of omental
702 milky spots and milky spot macrophages by intraperitoneal administration of a
703 streptococcal preparation, OK-432. *Cancer Research* 1992, 52:5400–5402.
- 704 33. Litbarg NO, Gudehithlu KP, Sethupathi P, Arruda JAL, Dunea G, Singh AK: Activated
705 omentum becomes rich in factors that promote healing and tissue regeneration. *Cell*
706 *Tissue Res* 2007, 328:487–497.
- 707 34. Rangel-Moreno J, Moyron-Quiroz JE, Carragher DM, Kusser K, Hartson L, Moquin A,
708 Randall TD: Omental Milky Spots Develop in the Absence of Lymphoid Tissue-Inducer
709 Cells and Support B and T Cell Responses to Peritoneal Antigens. *Immunity*, Elsevier
710 Ltd, 2009, 30:731–743.
- 711 35. Wijffels JF, Hendrickx RJ, Steenbergen JJ, Eestermans IL, Beelen RH: Milky spots in
712 the mouse omentum may play an important role in the origin of peritoneal
713 macrophages. *Res Immunol* 1992, 143:401–409.
- 714 36. Shimotsuma M, Takahashi T, Kawata M, Dux K: Cellular subsets of the milky spots in

- 715 the human greater omentum. *Cell Tissue Res* 1991, 264:599–601.
- 716 37. Cranshaw ML, Leak LV: Milky spots of the omentum: a source of peritoneal cells in the
717 normal and stimulated animal. *Arch Histol Cytol* 1990, 53 Suppl:165–177.
- 718 38. Beelen RH, Fluitsma DM, Hoefsmit EC: The cellular composition of omentum milky
719 spots and the ultrastructure of milky spot macrophages and reticulum cells. *J*
720 *Reticuloendothel Soc* 1980, 28:585–599.
- 721 39. Krist LF, Eestermans IL, Steenbergen JJ, Hoefsmit EC, Cuesta MA, Meyer S, Beelen
722 RH: Cellular composition of milky spots in the human greater omentum: an
723 immunochemical and ultrastructural study. *Anat Rec* 1995, 241:163–174.
- 724 40. Mironov VA, Gusev SA, Baradi AF: Mesothelial stomata overlying omental milky spots:
725 scanning electron microscopic study. *Cell Tissue Res* 1979, 201:327–330.
- 726 41. Dux K, Janik P, Szaniawska B: Kinetics of proliferation, cell differentiation, and IgM
727 secretion in the omental lymphoid organ of B10/Sn mice following intraperitoneal
728 immunization with sheep erythrocytes. *Cellular Immunology*, Elsevier, 1977, 32:97–
729 109.
- 730 42. Krist LF, Kerremans M, Broekhuis-Fluitsma DM, Eestermans IL, Meyer S, Beelen RH:
731 Milky spots in the greater omentum are predominant sites of local tumour cell
732 proliferation and accumulation in the peritoneal cavity. *Cancer Immunol Immunother*
733 1998, 47:205–212.
- 734 43. Green JA, Williams AE: The relationship between inflammatory responses and WBP1
735 tumour cell attachment to the rat omentum. *Eur J Cancer* 1978, 14:1153–1155.
- 736 44. Sorensen EW, Gerber SA, Sedlacek AL, Rybalko VY, Chan WM, Lord EM: Omental
737 immune aggregates and tumor metastasis within the peritoneal cavity. *Immunol Res*
738 2009, 45:185–194.
- 739 45. Tsujimoto H, Takhashi T, Hagiwara A, Shimotsuma M, Sakakura C, Osaki K, Sasaki S,

740 Shirasu M, Sakakibara T, Ohyama T: Site-specific implantation in the milky spots of
 741 malignant cells in peritoneal dissemination: immunohistochemical observation in mice
 742 inoculated intraperitoneally with bromodeoxyuridine-labelled cells. *Br J Cancer*, Nature
 743 Publishing Group, 1995, 71:468.

744 46. Tsujimoto H, Hagiwara A, Shimotsuma M, Sakakura C, Osaki K, Sasaki S, Ohyama T,
 745 Ohgaki M, Imanishi T, Yamazaki J, Takahashi T: Role of milky spots as selective
 746 implantation sites for malignant cells in peritoneal dissemination in mice. *J Cancer Res*
 747 *Clin Oncol* 1996, 122:590–595.

748 47. Nieman KM, Kenny HA, Penicka CV, Ladanyi A, Buell-Gutbrod R, Zillhardt MR,
 749 Romero IL, Carey MS, Mills GB, Hotamisligil GS, Yamada SD, Peter ME, Gwin K,
 750 Lengyel E: Adipocytes promote ovarian cancer metastasis and provide energy for rapid
 751 tumor growth. *Nat Med* 2011, 17:1498–1503.

752 48. Takemori N, Hirai K, Onodera R, Saito N, Namiki M: Light and electron microscope
 753 study of splenoportal milky spots in New Zealand black mice: comparison between
 754 splenoportal milky spots and aberrant spleens. *J Anat* 1995, 186 (Pt 2):287–299.

755 49. Yu D, Wolf JK, Scanlon M, Price JE, Hung MC: Enhanced c-erbB-2/neu expression in
 756 human ovarian cancer cells correlates with more severe malignancy that can be
 757 suppressed by E1A. *Cancer Research* 1993, 53:891–898.

758 50. Delves P, Martin S, Burton D, Roitt I: *Roitt's Essential Immunology*. 11th ed. Wiley-
 759 Blackwell, 2006.

760 51. Thévenaz P, Ruttimann UE, Unser M: A pyramid approach to subpixel registration
 761 based on intensity. *IEEE Trans Image Process* 1998, 7:27–41.

762 52. Weinberg DF, Baldo-Correa E, Lenzi HL, Borojevic R: *Schistosoma mansoni*:
 763 peritoneal plasmacytogenesis and polypoid transformation of mesenteric milky spots in
 764 infected mice. *Exp Parasitol* 1992, 74:408–416.

- 765 53. Dirat B, Bochet L, Dabek M, Daviaud D, Dauvillier S, Majed B, Wang YY, Meulle A,
766 Salles B, Le Gonidec S, Garrido I, Escourrou G, Valet P, Muller C: Cancer-associated
767 adipocytes exhibit an activated phenotype and contribute to breast cancer invasion.
768 Cancer Research 2011, 71:2455–2465.
- 769 54. Wyckoff J, Wang W, Lin EY, Wang Y, Pixley F, Stanley ER, Graf T, Pollard JW, Segall
770 J, Condeelis J: A paracrine loop between tumor cells and macrophages is required for
771 tumor cell migration in mammary tumors. Cancer Research 2004, 64:7022–7029.
- 772 55. Qian B-Z, Pollard JW: Macrophage diversity enhances tumor progression and
773 metastasis. Cell 2010, 141:39–51.
- 774 56. Tlsty TD, Coussens LM: Tumor stroma and regulation of cancer development. Annu
775 Rev Pathol 2006, 1:119–150.
- 776 57. Coussens LM, Werb Z: Inflammation and cancer. Nature 2002, 420:860–867.
- 777 58. Robinson-Smith TM, Isaacsohn I, Mercer CA, Zhou M, Van Rooijen N, Husseinadeh
778 N, McFarland-Mancini MM, Drew AF: Macrophages Mediate Inflammation-Enhanced
779 Metastasis of Ovarian Tumors in Mice. Cancer Research 2007, 67:5708–5716.
- 780 59. Barbolina MV, Moss NM, Westfall SD, Liu Y, Burkhalter RJ, Marga F, Forgacs G,
781 Hudson LG, Stack MS: Microenvironmental regulation of ovarian cancer metastasis.
782 Stack MS, Fishman DA, editors. Boston, MA, Springer US, 2009, pp. 319–334.
- 783 60. Iwanicki MP, Davidowitz RA, Ng MR, Besser A, Muranen T, Merritt M, Danuser G, Ince
784 T, Brugge JS: Ovarian Cancer Spheroids Use Myosin-Generated Force to Clear the
785 Mesothelium. Cancer Discovery 2011, 1:144–157.
- 786 61. Branco-Price C, Zhang N, Schnelle M, Evans C, Katschinski DM, Liao D, Ellies L,
787 Johnson RS: Endothelial cell HIF-1 α and HIF-2 α differentially regulate metastatic
788 success. Cancer Cell 2012, 21:52–65.
- 789 62. Neiva KG, Zhang Z, Miyazawa M, Warner KA, Karl E, Nör JE: Cross talk initiated by

- endothelial cells enhances migration and inhibits anoikis of squamous cell carcinoma cells through STAT3/Akt/ERK signaling. *Neoplasia* 2009, 11:583–593.
63. H C Hollingsworth ECKSMSMLRMJM: Tumor angiogenesis in advanced stage ovarian carcinoma. *The American Journal of Pathology*, American Society for Investigative Pathology, 1995, 147:33.
64. Mixter RL: On macrophagal foci (“milky spots”) in the pleura of different mammals, including man. *American Journal of Anatomy*, Wiley Online Library, 1941, 69:159–186.
65. Bozza PT, Viola J: Lipid droplets in inflammation and cancer. *Prostaglandins* 2010.
66. Pond CM: Adipose tissue: quartermaster to the lymph node garrisons. *Biologist* (London) 2000, 47:147–150.
67. Pond CM, Mattacks CA: Interactions between adipose tissue around lymph nodes and lymphoid cells in vitro. *J Lipid Res* 1995, 36:2219–2231.
68. Walter M, Liang S, Ghosh S, Hornsby PJ, Li R: Interleukin 6 secreted from adipose stromal cells promotes migration and invasion of breast cancer cells. *Oncogene* 2009, 28:2745–2755.
69. Tan J, Buache E, Chenard MP, Dali- Youcef N, Rio MC: Adipocyte is a non-trivial, dynamic partner of breast cancer cells. *International journal of developmental biology*, Departamento de Biología Celular e Histología, 2011, 55:851–859.
70. Kim JH, Kim K-Y, Jeon JH, Lee SH, Hwang J-E, Lee JH, Kim KK, Lim J-S, Kim KI, Moon E-Y, Lee HG, Ryu J-H, Yang Y: Adipocyte culture medium stimulates production of macrophage inhibitory cytokine 1 in MDA-MB-231 cells. *Cancer Lett* 2008, 261:253–262.
71. Paget S: The distribution of secondary growths in cancer of the breast. 1889. *The Lancet* 1889, 133:571–573.
72. Kenny PA, Bissell MJ: Tumor reversion: correction of malignant behavior by

- 815 microenvironmental cues. *Int J Cancer* 2003, 107:688–695.
- 816 73. Bissell MJ, Radisky DC, Rizki A, Weaver VM, Petersen OW: The organizing principle:
817 microenvironmental influences in the normal and malignant breast. *Differentiation* 2002,
818 70:537–546.
- 819 74. Nicolson GL: Organ specificity of tumor metastasis: role of preferential adhesion,
820 invasion and growth of malignant cells at specific secondary sites. *Cancer Metastasis*
821 *Rev* 1988, 7:143–188.
- 822 75. Fidler IJ: The pathogenesis of cancer metastasis: the “seed and soil” hypothesis
823 revisited. *Nat. Rev. Cancer*. 2003, pp. 453–458.
- 824 76. Hart IR, Fidler IJ: Role of Organ Selectivity in the Determination of Metastatic Patterns
825 of B16 Melanoma. *Cancer Research* 1980.
- 826 77. Sugarbaker EV: Cancer metastasis: a product of tumor-host interactions. *Curr Probl*
827 *Cancer* 1979, 3:1–59.

828

829

830 **Figure Legends**

831 **Figure 1. The relative locations of the main depots of peritoneal adipose. A:** Left view of
832 the peritoneal cavity of a B6 mouse, exposed via a ventral incision. This gross anatomic
833 dissection shows the relative location of four of the five primary sources of peritoneal fat.
834 Beginning at the top center and moving clockwise are: the omentum (OM; outlined) located
835 over the stomach and spleen, the gonadal fat (GF) surrounding the left ovary (ov), the uterine
836 fat (UF) attached to the uterine horns (uh) and the mesentery (MY) attached to the small
837 intestine (si). **B:** The fifth source of peritoneal adipose is the splenoportal fat, which can be
838 exposed by lifting the spleen with forceps (SP; outlined). **C:** The mouse omentum shown
839 dissected free from the pancreas and exposed here to improve visualization. Although
840 analogous to the human omentum in composition and tissue architecture, in mice the
841 omentum consists of a single ribbon of fat attached to the pancreas. **D:** Five sources of
842 peritoneal fat excised to show relative size. From left to right: splenoportal fat, omentum,
843 gonadal fat, uterine fat and mesentery (with attached mesenteric root).

844 **Figure 2. Ovarian cancer cells specifically colonize peritoneal adipose that contains**
845 **milky spots. A:** B6 mice were injected i.p. with either PBS as a control (*upper panels*) or
846 1×10^6 ID8 murine ovarian cancer cells (*lower panels*). At 7 dpi, tissues were excised for
847 histologic evaluation. In control tissues (*upper panels*) milky spots (MS) are seen
848 interspersed among adipocytes (A) in the omental and splenoportal fat. In contrast, no milky
849 spots were detected in the uterine fat, gonadal fat and mesentery, each composed mostly of
850 adipocytes (with occasional vessels being observed). After ID8 cell injection (*lower panels*),
851 large foci of cancer cells intermixed with immune cells were observed within milky spots in
852 the omentum and splenoportal fat (outlined in yellow). In contrast, ID8 cancer cells were not
853 observed in the uterine fat, gonadal fat or mesentery. The scale bar is the same for all

854 images and denotes 50 μm . **B:** Nude mice were injected i.p. with 1×10^6 SKOV3ip.1 human
855 ovarian cancer cells. At 7dpi, omenta and splenoportal fat were excised for histological
856 evaluation. Sections were evaluated by H&E staining. The presence of epithelial (cancer)
857 cells within the lesions was confirmed by IHC detection of cytokeratin using a pan-cytokeratin
858 antibody. IHC using an IgG isotype antibody for pan-cytokeratin was used as a control for
859 staining specificity. The scale bar is the same for all images and denotes 100 μm .

860 **Figure 3. Milky spot-containing adipose tissues show enhanced ability to stimulate**
861 **directed migration.** Transwell migration assays were used to test the ability of the omentum
862 and other peritoneal adipose tissues to produce soluble factors that promote the directed
863 migration of ovarian cancer cells. **A:** Schematic description of experimental design. **B: Top:**
864 Depiction of migration assay setup. Cancer cells were placed in the upper chamber of the
865 transwell apparatus. The chemoattractant media, with or without starved tissue, was placed
866 in the lower chamber as indicated. **Bottom:** Representative membranes from ID8 migration
867 assays. **C:** Quantitation of ID8 (*left*) and SKOV3ip.1 (*right*) cell migration in response to
868 factors produced by omenta harvested from CD-1 mice. Conditions are those illustrated in
869 Panel B, where SF denotes serum free media where CSF denotes conditioned serum and
870 SOM denotes starved omentum. **D:** Quantitation of ID8 (*left*) and SKOV3ip.1 (*right*) cell
871 migration in response to factors produced by omenta harvested from B6 and Nude mice. **E:**
872 Migration assay of ID8 cells toward serum-free media conditioned for 24 hr by tissue
873 equivalents of omenta (OM), splenoportal fat (SP), uterine fat (UF) and mesentery (MY)
874 harvested from B6 mice. $n=5$ for all conditions. $*p<0.05$, $***p<0.001$.

875 **Figure 4. An alternative protocol for labeling milky spots in mouse omenta. A:** A rare
876 example of a whole mount of a B6 omentum with clear milky spot labeling after carbon
877 staining. Scale bar = 1.0 mm. **B:** A more typical case of a B6 omentum ineffectively stained

878 with several carbon plaques (red arrows) obstructing milky spot visualization. Scale bar = 1.0
879 mm. **C:** As an alternative to carbon labeling, we developed a method wherein naive mouse
880 omenta were paraffin-embedded, sectioned at 4 μ m and stained with Giemsa. Dark staining
881 regions denote dense areas of immune aggregates. **D:** Image of omental tissue section
882 stained with Giemsa. Milky spots are indicated with black arrows. **E:** Image of omental tissue
883 section adjacent to D, stained with H&E. **F:** Image of omental tissue section adjacent to E,
884 evaluated by IHC using anti-CD45 antibody to identify lymphocytes within the milky spot
885 structure. The scale bar is the same for D-F and denotes 100 μ m. **G:** Mask of omentum
886 section (same as C) processed to show milky spots specifically converted to pure black
887 pixels. **H:** Mask of omentum section (same as C) processed to show the entire area of the
888 omentum converted to pure black pixels. The scale bar is the same for C, G and H and
889 denotes = 1.0 mm.

890 **Figure 5. The milky spot volume of the omentum is not affected to the host's immune**
891 **status.** Giemsa-stained sections of omenta harvested from B6, Nude, Rag1, Igh6 and BN
892 XID mice were processed, sectioned, Geimsa stained and imaged to allow for automated
893 quantitation of milky spot and whole omenta area on each section (as described in the
894 Materials and Methods). Volumes were calculated by multiplying the area of each section by
895 4 μ m and summing sections from individual omenta. **A:** Milky spot volume per omentum. **B:**
896 Total volume of the whole omentum. **C:** Milky spot volume as a percentage of the total
897 omentum volume. For each mouse strain, milky spot and omental volumes were determined
898 for 5 independent animals. Using one-way ANOVA, no measurements were statistically
899 different among any of the mouse strains.

900 **Figure 6. Colonization of omental milky spots by ovarian cancer cells is not dependent**
901 **on the host immune status. A:** To test the possibility that the lymphocyte population of the

902 milky spots has a quantitative effect on ovarian cancer cell colonization, mice with
903 deficiencies in T cells, B cells and/or NK cells were injected i.p. with either PBS (control;
904 *upper panel*) or 1×10^6 ovarian cancer cells (*lower panel*). B6 mice were injected with
905 syngeneic ID8 cells. Nude, Rag1 and BN XID mice were injected with human SKOV3ip.1
906 cells. Omenta were collected at 7 dpi and were processed for histology (using H&E staining).
907 Cancer cell foci within immune aggregates are outlined. The scale bar is the same for all
908 images and denotes 50 μm . **B:** IHC with a pan-cytokeratin antibody was used to confirm that
909 the lesions observed in milky spots of Nude, Rag1 and BN XID mice at 7 dpi were composed
910 of SKOV3ip.1 cells, tissue sections were immunostained with pan-cytokeratin antibody. As a
911 control for nonspecific background staining, omental tissue from Nude mice injected with PBS
912 was also evaluated by IHC using a pan-cytokeratin antibody (*far left panel*). To control for
913 antibody specificity, IHC with an isotype IgG for the pan-Cytokeratin antibody was used to
914 evaluate omental tissues from mice injected with SKOV3ip.1 cells. Samples from 5
915 independent animals were evaluated for each condition. The scale bar is the same for all
916 images and denotes 100 μm .

917 **Figure 7. Adipocyte area of the omentum decreases during the timecourse ovarian**
918 **cancer growth. A:** The first panel shows a representative H&E stained section of an
919 omentum from a naive B6 mouse. Milky spots are seen within adipose at the tissue
920 periphery. The four subsequent panels show representative images of omental tissues
921 harvested from B6 mice at 1, 3, 6 and 9 weeks post injection. The scale bar is the same for
922 all images and denotes 200 μm . **B:** Quantitation of adipocyte area from H&E images.
923 Reported values are percent adipocyte area normalized to whole omental area. Data at each
924 time point is based on five independent animals. A linear regression of the data points
925 indicates a slope significantly deviant from zero ($p < 0.0001$) with $R^2 = 0.8145$.

926

927 **Supplemental Figure 1. Representative histology of peritoneal fat deposits in naive B6**
928 **mice.** Milky spots (MS) are seen at the tissue periphery adjacent to adipocytes (A) in the
929 omentum and splenoportal fat of H&E stained tissue sections. Milky spots are not seen in
930 H&E stained tissue sections from uterine fat, gonadal fat and mesentery. Arrows indicate
931 blood vessels. The scale bar is the same for all images and denotes 50 μ m.

932 **Supplemental Figure 2. Evaluation of tissue integrity and function of tissues**
933 **maintained in ex vivo culture. Left column:** The effect of *ex vivo* culture on tissue integrity
934 and cellularity was determined by histologic evaluation of freshly excised tissues. **Middle**
935 **column:** Histology of tissues maintained for 24 hr in DMEM/F12 with 20% FCS followed by a
936 24 hr culture in DMEM/F12 with 20% FCS. **Right column:** To assess tissue viability and
937 function under *ex vivo* conditions, the amount of IL-6 in the SF culture media was determined
938 at 24 hr intervals. As a control, the amount of IL-6 secreted by tissues maintained in media
939 containing 20% FCS was determined in parallel. The relative amount of IL-6 at each
940 timepoint is the ratio of the measured IL-6 concentration to the IL-6 concentration in the
941 control group. The scale bar is the same for all images and denotes 50 μ m. *** $p < 0.001$.

942 **Supplemental Figure 3. Visualization of omental milky spots using Giemsa staining.**
943 Omenta from naive BL6, Nude, Rag1, Igh6 and BN XID mice were excised, sectioned and
944 stained with Giemsa. **Left:** Whole omentum image, dark blue staining regions coincide with
945 milky spot structures. **Right:** At higher magnification, milky spots are seen as dark-staining
946 regions of immune cells.

947 **Supplemental Figure 4. Three-dimensional rendering of mouse omentum.** Giemsa
948 stained sections of a naive B6 omentum were stacked, aligned and projected into a 3D
949 rendering of the whole tissue. This false colored image depicts milky spots as white and
950 stromal architecture as blue.

951 **Supplemental Methods. Macros used for quantification of omental tissue components.**

952

953 **Milky Spot Area Quantification of Giemsa-Stained Tissue**

954 run("8-bit");

955 run("Invert LUT");

956 run("Color Balance...");

957 setMinAndMax(146, 224);

958 call("ij.ImagePlus.setDefault16bitRange", 0);

959 run("Apply LUT", "stack");

960 run("Make Binary", " ");

961 run("Invert LUT");

962 setAutoThreshold("Default");

963 //run("Threshold...");

964 setThreshold(24, 255);

965 run("Convert to Mask", " ");

966 run("Analyze Particles...", "size=0-Infinity circularity=0.00-1.00 show=Masks display

967 summarize stack");

968

969 **Omentum Area Quantification of Giemsa-Stained Tissue**

970 run("8-bit");

971 //run("Brightness/Contrast...");

972 setMinAndMax(200, 255);

973 call("ij.ImagePlus.setDefault16bitRange", 0);

974 setAutoThreshold("Default");

975 //run("Threshold...");

976 setThreshold(0, 247);

977 setThreshold(0, 247);

978 run("Convert to Mask", " ");

979 run("Find Edges", "stack");

980 run("Convert to Mask", " ");

981 run("Convert to Mask", " ");

982 run("Fill Holes", " ");

983 run("Analyze Particles...", "size=25-Infinity circularity=0.00-1.00 show=Masks display include

984 summarize stack");

985

986 **Non-Adipocyte Area Quantification of H&E-Stained Tissue**

987 run("8-bit");

988 //run("Brightness/Contrast...");

989 setMinAndMax(161, 255);

990 call("ij.ImagePlus.setDefault16bitRange", 0);

991 //run("Threshold...");

992 setAutoThreshold("Default");

993 setThreshold(0, 195);

994 run("Analyze Particles...", "size=25-Infinity circularity=0.00-1.00 show=Masks display

995 summarize");

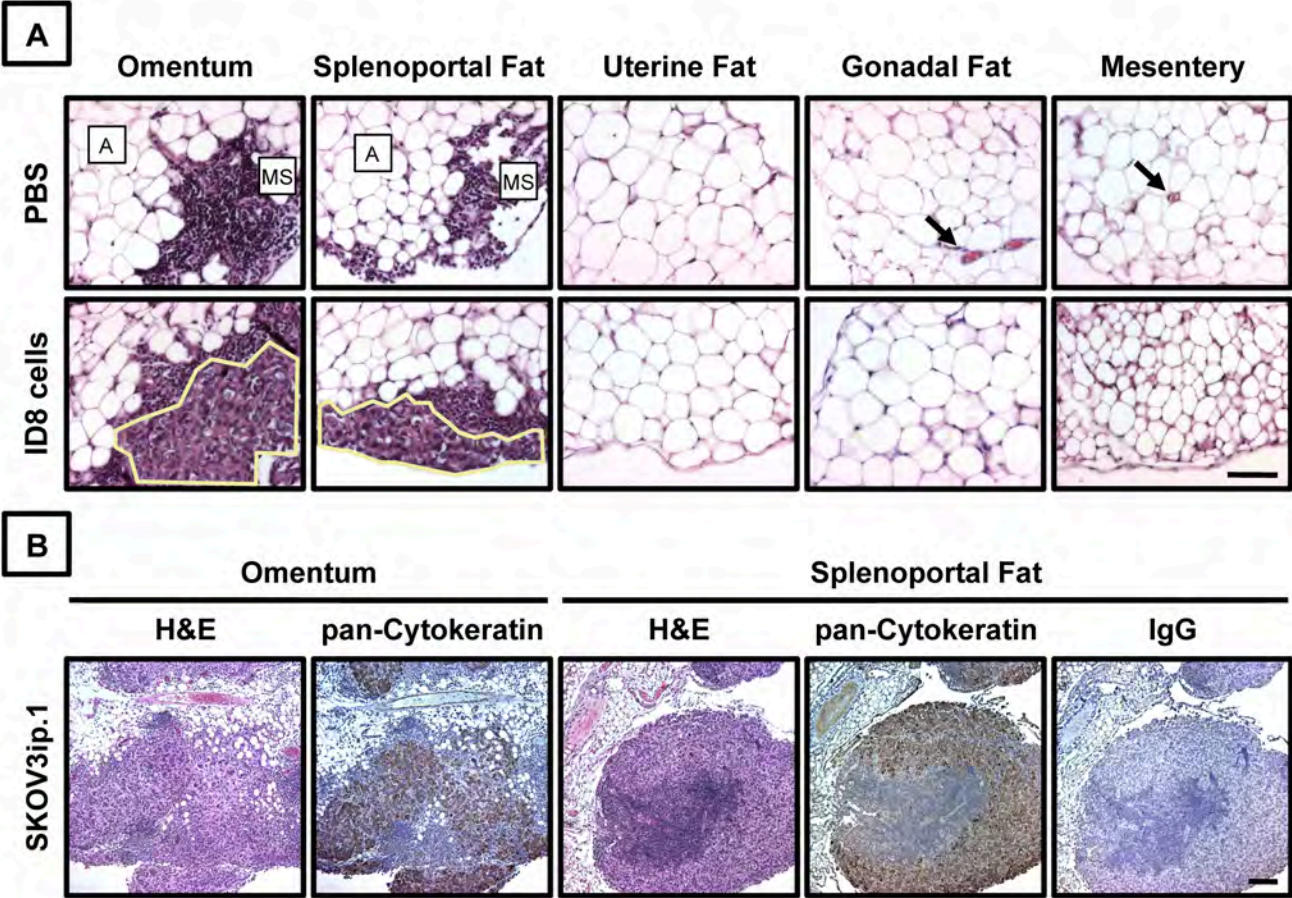
996

997 **Omentum Area Quantification of H&E-Stained Tissue**

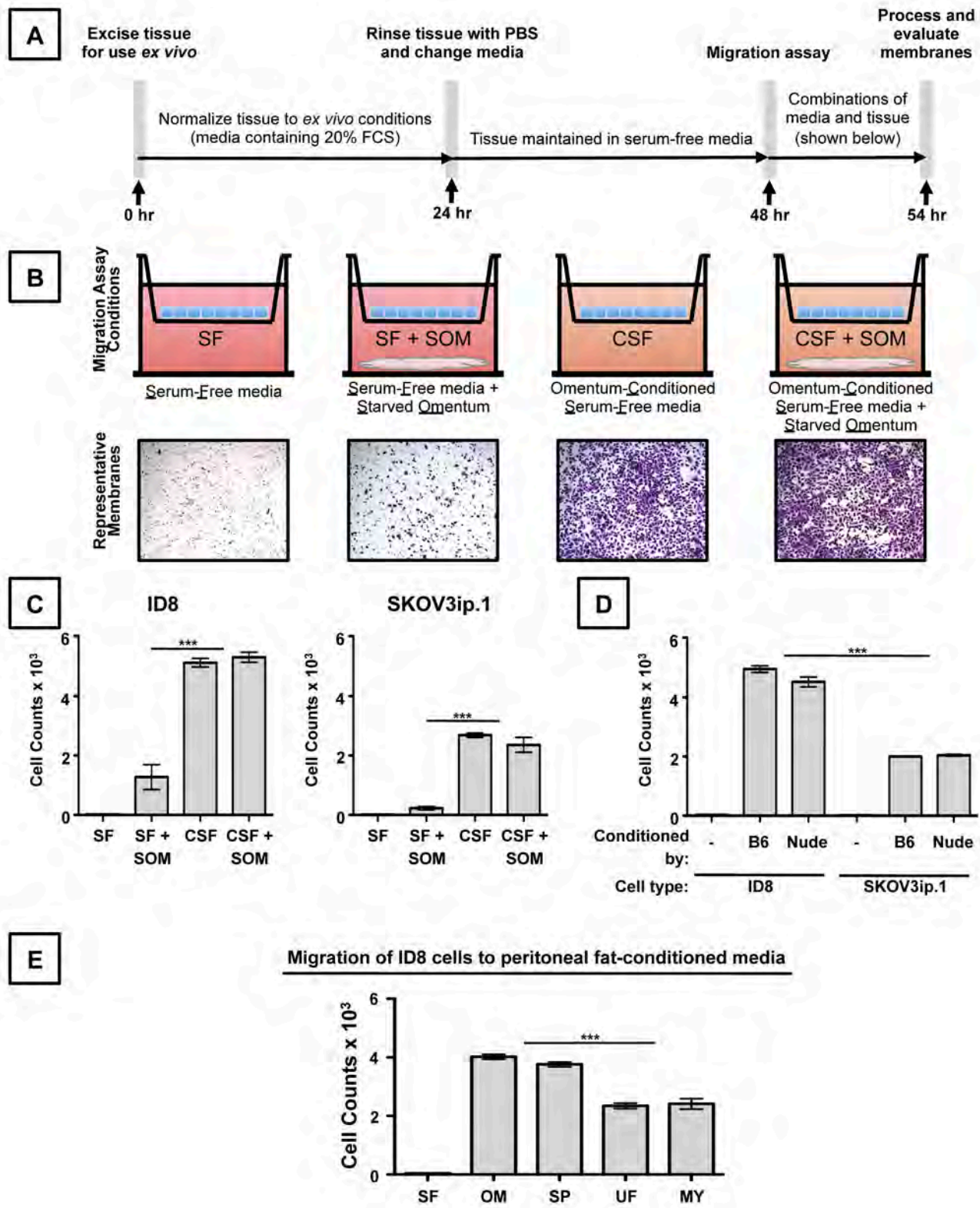
998 run("8-bit");

```
999 //run("Brightness/Contrast...");
1000 setMinAndMax(243, 255);
1001 call("ij.ImagePlus.setDefault16bitRange", 0);
1002 setAutoThreshold("Default");
1003 //run("Threshold...");
1004 setThreshold(0, 248);
1005 run("Analyze Particles...", "size=25-Infinity circularity=0.00-1.00 show=Masks display include
1006 summarize");
1007
1008
```

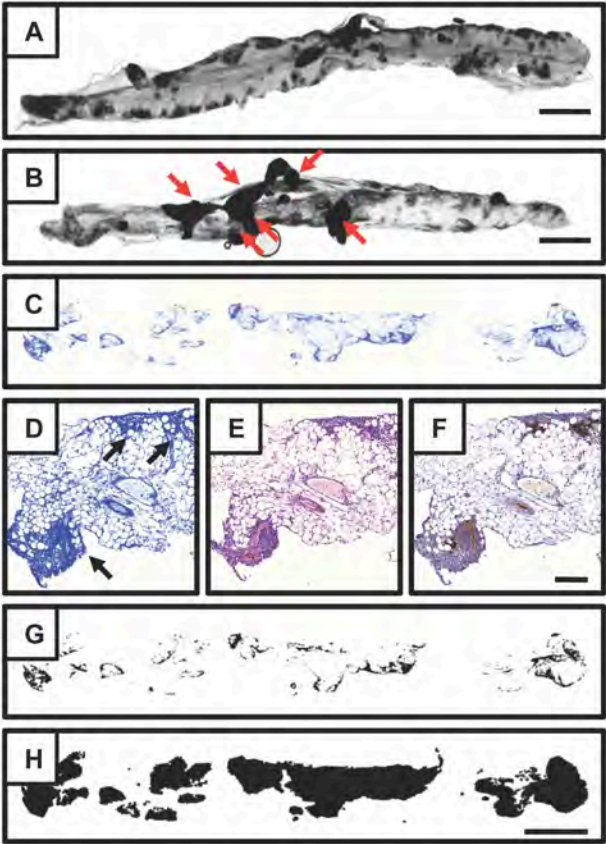
Clark and Krishnan, *et al.* Figure 2



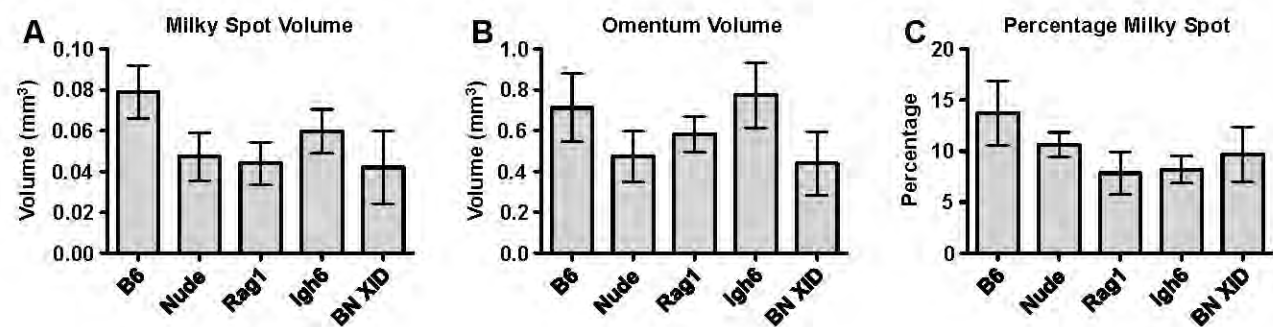
Clark and Krishnan, *et al.* Figure 3



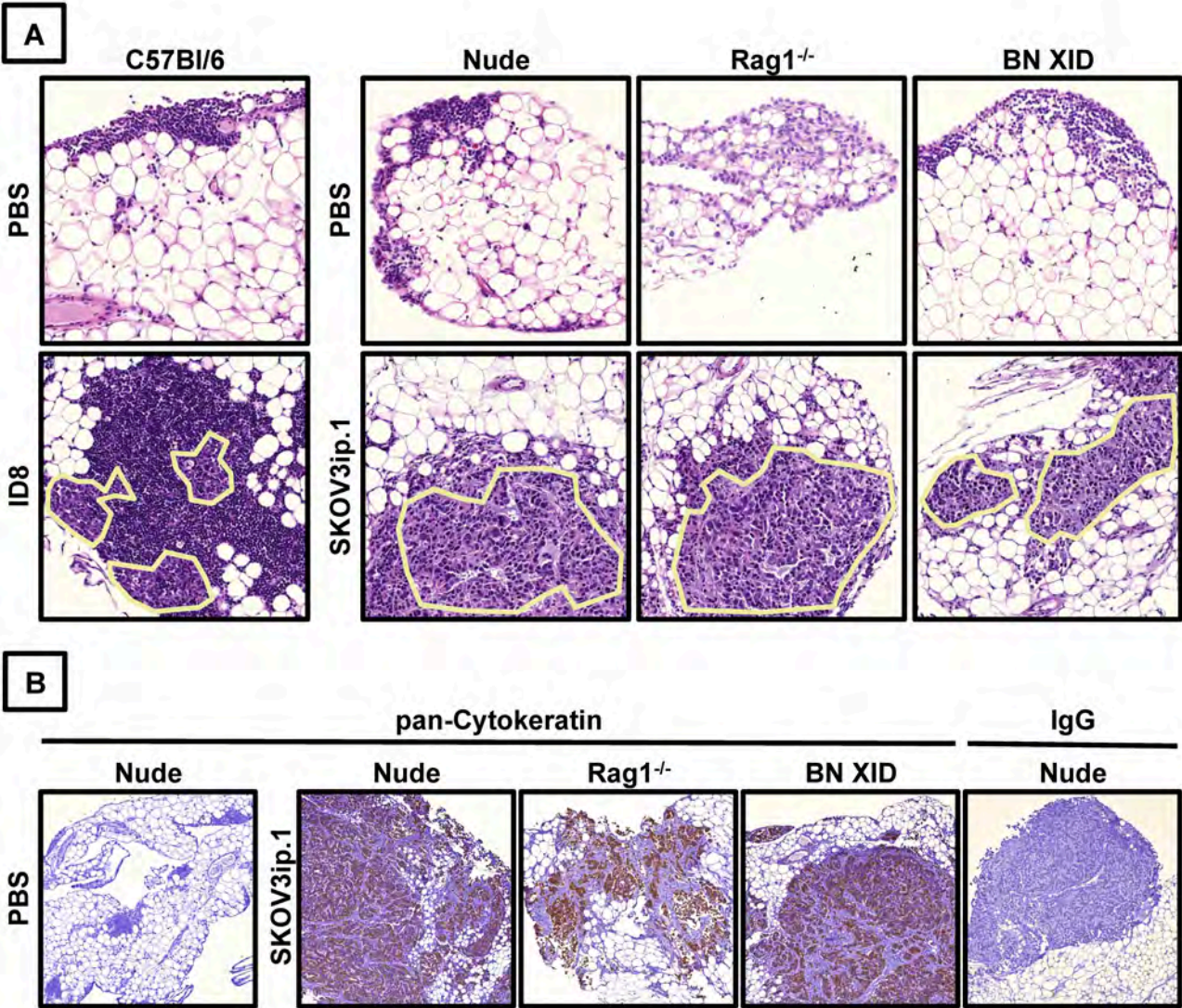
Clark and Krishnan, *et al.* Figure 4



Clark and Krishnan, *et al.* Figure 5



Clark and Krishnan, *et al.* Figure 6



Clark and Krishnan, *et al.* Figure 7

